Computational Modeling of Mechanosensitive Neuron Populations in the Human Tongue During Oral Processing

A dissertation presented to
the faculty of the School of Engineering and Applied Science
University of Virginia

In partial fulfillment
of the requirements for the degree of
Doctor of Philosophy in Systems Engineering

Merat Rezaei
Advisor: Gregory J. Gerling
June, 2024

APPROVAL SHEET

This Dissertation

is submitted in partial fulfillment of the requirements for the degree of

Doctor of Philosophy

Author: Merat Rezaei

Advisor: Gregory J. Gerling

Committee Member: Matthew Bolton

Committee Member: Afsaneh Doryab

Committee Member: Stephen Baek

Committee Member: Brian Guthrie

Accepted for the School of Engineering and Applied Science:

Jennifer L. West, School of Engineering and Applied Science

Graduation: August, 2024

To my parents, brother, and friends, for their unwavering support.

To my advisor, Professor Greg Gerling, whose mentorship and dedication to my success have left an indelible mark on my life.

Abstract

When placed in the oral cavity, we almost immediately recognize the physical characteristics of food, such as its compliance, surface roughness, and geometry. Moreover, we can instinctively judge the amount of mastication necessary to break a food down into a bolus ready to be swallowed. The perceptual encoding of food during stages of oral processing is of significant importance in the research of food science, but efforts to reproduce percepts such as 'firmness,' 'smoothness,' and 'thickness,' via the modulation of tribological and rheological properties have been especially evasive. Furthermore, these efforts have overlooked roles of sensory and proprioceptive feedback from the tongue. In this work, we developed predictive computational models that clarify the interplay of subtypes of sensory neural afferents, and their capacity to contribute to the neural encoding of stimulus diameter, contact geometry, and relative position. First, we employed differential equation models that abstract the neural biophysics in generating mechanosensitive currents and spike firing. Second, we built models of afferent population, varying in density, that encode spatial elements of stimuli such as diameter and contact geometry. Moreover, we leveraged machine learning approaches to classify stimulus spatial elements through their elicited afferent population responses. Our efforts aim in the longer-term development of a computational platform to decode stimulus compliance, surface roughness, and lateral motion, via population response profiles of mechanosensitive afferents, as more layers of complexity in terms of stimulus contact mechanics with the simulated tongue become available. Furthermore, the grand aim of this effort is to provide the foundational steps in creating a computational platform, which can decode complex percepts, e.g. firmness, smoothness, and thickness.

Contents

Overview of aims....6
Significance and Contribution....8
Background....10
Aim 1. Differentiate unique contributions of neural afferent subtypes in encoding features of simulated food stimuli during the first bite stage of oral processing....12
Introduction....13
Methods....14
Results....18
Discussion....22
Aim 2: Develop an afferent population model to encode the shape, size, position, and motion of simulated food stimuli during the first bite stage of oral processing....23
Introduction....24
Methods....27
Results....34
Discussion....40
Overall conclusions and future work....41
Summary of Findings....41
Aim 1....41
Aim 2....42
Implications for Food Science and Industry....43
Future Work....43
Incorporation of Additional Afferent Subtypes....43
Exploration of Complex Stimuli....43
Application to Oral Processing Disorders....44
Publications....44
References....45

Overview of aims

The objective of this effort is to develop predictive computational models that will uncover the utility of how sensory neural afferent types signal the mechanical properties of simulated stimuli during oral processing. We are particularly interested in clarifying the interplay of various afferent subtypes during modulation of stimulus stress magnitude and vibrational frequencies, and their capacity to uniquely contribute to the neural encoding of various stimulus geometries, diameters, and positions over time. This clarification will be conducive to our understanding of the cues that are critical in informing higher level physical attributes of food such as compliance, surface roughness, and movement velocity.

When we eat something, we have an almost immediate perception of its characteristics such as compliance, surface roughness, size, and shape. Moreover, we instinctively know the amount of mastication necessary to break the food down into a bolus that is ready to be swallowed, by tracking its tribological behavior, compliance, and geometry during oral processing. The currently accepted paradigm for creating new food products that are optimized for consumer preferences, is to vary their chemical composition through trial and error, in such a way that their mechanical properties are measurably modulated. Then, participants are asked to intermittently evaluate a food's perceptual properties such as 'firmness,' 'smoothness,' and 'thickness' during its breakdown, until it is swallowed. Beyond percepts alone, facial electromyography (EMG) can simultaneously measure chewing forces, jaw muscle activity, and motor movement. However, these motor-oriented efforts overlook roles of sensory and proprioceptive feedback from the tongue, and do not provide a computational platform for creating new food products due to innumerable possible variations in their chemical composition, which can be evaluated perceptually. **Our central hypothesis** is that computational models of populations of mechanosensitive afferents of the tongue can be built to replicate important sensory inputs, and thereby differentiate the aforementioned food stimulus characteristics over the spatiotemporal course of their food breakdown. In the long term, this approach may help curtail the need for incessant, one-off perceptual evaluation of foods, by reducing the input domain to subsets of food stimuli. **We addressed the central hypothesis by** differentiating the unique

contributions of afferent subtypes in encoding food stimulus features and building an afferent population model capable of encoding compliance, size, shape, position, and motion of food stimuli. Methods include i) employed differential equation models that represent a leaky-integrate-and-fire abstraction of a neuron, of 2 afferent subtypes (of slowly-adapting, rapidly-adapting) to generate mechanotransduction currents and spike firing, ii) developed an afferent population model of 25 to 5000 units (44% slowly-adapting, 56% rapidly-adapting) and modulating their relative density and spatial configuration to encode geometry, position, and size of stimuli, and leveraging machine learning approaches such as Random Forest classification and regression, to predict stimulus input parameters, according to population spike firing profiles. These methods were used to address two aims:

Aim 1: Differentiate unique contributions of neural afferent subtypes in encoding features of simulated food stimuli.

We employed computational models of neural afferents using differential equations that represent a leaky-integrate-and-fire abstraction of a neuron, to generate mechanotransduction currents and spike firing patterns, distinct for slowly-adapting and rapidly-adapting subtypes, that encode physical features of simulated food stimuli. These are biophysical computational models, and primarily differ from each other in time constant settings which represent the inactivation period of their mechanotransduction currents. As input to these models, we simplified the contact mechanics of stimuli derived from mechanical measurements in the literature, focused upon attributes of material compliance and surface roughness. Ramp-and-hold stimuli simulate forces during mastication and swallowing of foodstuffs. Periodic stimuli mimic behavior of food sliding over the tongue. Rather than using a finite element model to simulate the stimulus to skin interactions, we generated representative spatiotemporal stress traces over time to be delivered to simulated receptive fields of the afferent subtypes in normal directions.

Aim 2: Develop an afferent population model to decode the geometry and diameter of simulated food stimuli.

We developed a population model of slowly-adapting (SA) and rapidly-adapting (RA) mechanosensitive afferents, varying in density, and receptive field sizes inspired by human neurophysiological data of the tongue and glabrous skin of the hand. The results indicate that spike firing response profiles of a population of 1000 afferents (44% SA, 56% RA) on 50 x 25 mm cross-sectional area of the tongue, can reliably differentiate stimulus geometry across a wide range of diameters from 0.05 mm to 20 mm, while remaining insensitive to changes in stimulus position due to high afferent density. Machine learning techniques were employed to make predictions of these high-level spatial attributes, based solely on the total number of afferents recruited, and total number of spikes elicited by a particular stimulus. Following efforts to mitigate risks of overfitting, using 5-fold cross-validation of training data, we achieved a 90.85% mean accuracy rate in geometry classification, and a 0.92 mean-squared error (R^2 = 0.98) for diameter regression using a Random Forest algorithm. Classification of relative stimulus position yielded accuracy rates lower than chance (50%), verifying the population model's invariance to position modulation. This effort offers a foundational first step for building more complex mechanosensory models, affording the eventual encoding of stimulus compliance, surface roughness, and movement velocity, via their amalgamation with biomechanics of the human tongue.

Significance and Contribution

Due to discoveries regarding the detriment of foods high in sugar and fat content to our health, and thereby quality of life, shifting away from them has been an imperative direction in the food industry. However, maintaining equal levels of consumer satisfaction during this transition has been particularly evasive with synthetic fat and sugar substitutions that mimic the mechanical properties of the original. More specifically, while rigorous testing and iterative production of these newly engineered foods has been done to exactly replicate the rheological and tribological behaviors of their predecessors during oral processing,

reproducing mouthfeel percepts such as ‘thickness,’ ‘firmness,’ and ‘smoothness’ have been considerably more difficult. This has not been aligned with consumer preferences. Relationships between sensory perception and oral tribology [1], and jaw muscle activities using electromyography [2] are valuable, but they do not address the neural encoding of food stimuli, an intrinsic and vital aspect of perceptual realization. While there are other types of neural receptors in the tongue that have important contributions to sensory perception, such as nociceptors (pain detection), thermal receptors, and taste receptors, in this work we focus on a subset of low threshold mechanoreceptors specialized for informing the physical properties of stimuli, which is inherently valuable. Our findings have important implications for the food industry, particularly in the design and development of new food products that are optimized for specific consumer preferences, while mitigating the need for tedious psychophysical experimentation of foods during their mechanical breakdown. Additionally, the results of this research could inform interventions for individuals with oral processing impairments such as chronic xerostomia, and stroke victims who cannot determine when their food is ready to swallow.

Gap in the Knowledge Base. Herein, we develop predictive computational models that uncover the utility of how sensory neural afferent types signal the mechanical properties of food stimuli during oral processing, using biophysical models. To achieve this goal, we built a population model comprised of two afferent subtypes, capable of encoding geometry, diameter, and position of food stimuli, and used machine learning techniques to predict stimulus parameters, based on their afferent population responses. As research on the neurophysiology of the tongue is scarce, we faced certain limitations in terms of validating our models biologically. First, such computational models have never been built before for afferents in the tongue, let alone populations of mixed afferent subtypes. Moreover, we validated our individual computational models based on tongue microneurography data elicited from Von-Frey monofilaments.

Background

Mechanical attributes of food stimuli and their interrelations with sensory perception. A critical aspect of understanding consumer food selectivity and appeal to certain textures while avoiding others, lies in the interrelations between the physical and structural properties of food and how they are perceived during oral processing. As texture perception during oral processing is the emanation of output from multiple sensory modalities such as vision, hearing, and touch, it is particularly difficult to delineate what exact structural, mechanical, and surface properties of food evoke a particular percept [3]. A sensory method known as the Temporal Dominance of Sensation (TDS) has been used to build texture pathways to evaluate the dynamics of perceptions such as 'crispiness,' 'brittleness,' and 'stickiness' during various stages chewing solid foods [4], [5], [6], [7]. Through the modulation of microstructures in whey protein/k-carrageenan mixed gels, and thereby their mechanical attributes, others have demonstrated that sensory percepts of soft-solid foods can be generated over the course of the different phases of oral processing; first compression, first bite, mastication, and before swallowing [8]. Oral muscle activity and chewing frequency/duration have also been strongly correlated with the sensory perception of 'firmness' [2].

Single unit afferent subtypes in glabrous skin. A complex array of mechanosensory neurons enable us to detect objects that come into contact with our skin surface [9], [10], [11], [12]. In the glabrous skin of the mammalian hand, at least four distinct classes of mechanoreceptors, or afferents, have been discovered; each optimized for extracting particular attributes of an external stimulus. Slowly-adapting SAI afferents for normal indentation, slowly-adapting SAII afferents for skin stretch, rapidly-adapting RAI afferents for rapid skin displacement, and RAII afferents for vibration. The primary distinction between rapidly-adapting and slowly-adapting mechanoreceptors can be made in their spike firing patterns in response to a simple indenting stimulus. This stimulus will elicit a sustained response from the SA afferents for as long as it exists, contrary to how RA afferents transiently respond during its onset and offset periods, remaining quiescent for the steady-state phase.

Somatosensory feedback of the tongue. A technique known as microneurography affords the direct, single and multi-unit recordings from nerves in the peripheral nervous system, comprised of any nerve structure outside of the brain and spinal cord [12], [13]. Orofacial recordings from humans have identified multiple afferent classes, as well as their associated receptive field sizes, force detection thresholds, and innervation locations across the tongue and other intraoral structures [14], [15], [16], [17], [18]. Currently, there is concrete evidence for at least three classes in the lingual nerve; RAI and SAI, which terminate in the surface skin of the tongue, and proprioceptive afferents deep in the oral musculature. More recent efforts however, have indicated the possibility for the existence of more based on the non-supervised clustering of afferent calcium imaging responses in mouse tongue, including a type that exclusively responds to light, lateral stroking with a brush [19].

Computational modeling of SAI afferents. Each mechanoreceptor subtype has a specialized anatomical structure, known as end organs, that determine their responses to external stimuli. The SAI afferent's end organ is a cluster of what is termed a Merkel cell-neurite complex [20], [21]. With mechanical stimulation, Merkel-cell neurite complexes produce a generator current that is converted to action potentials, producing spikes. Predictive computational models have been used to synthesize these mechanotransduction currents arising from a normally indented ramp and hold stimulus, in the context of a finite element skin mechanics simulation. In response to this stimulus, a stress trace is passed to a generator function, which calculates the generator current for one Merkel cell-neurite complex. This generator current (Eq. 1) is comprised of three individual currents, a slowly inactivating (SI) current attributed to the Merkel cell, and rapidly inactivating (RI) and ultra-slowly inactivating (USI) currents arising from neurites. Finally, the generator current is used to compute the afferent spike timings using a leaky-integrate-and-fire model (LIF) (Eq. 2), a biophysical model which essentially solves a differential equation for the membrane potential, and produces a spike if it exceeds a certain biologically validated threshold, in this case $5\ mv$ [22], [23], [24]. Biophysical models of first order neurons are advantageous in comparison to stimulus dependent models, which directly fit the spike generation parameters to a

presented stimulus' position, velocity, acceleration, and jerk [25], [26]. The latter reduces the physiological relevance of the computational model to actual neural dynamics, and makes it highly dependent on parameter fitting to specific stimuli.

Population modeling of first order afferents. Reciprocal interpretation, a principle stating that the population response of a first order afferent can be approximated with recordings from a single fiber, provides the basis for simulating afferent populations [27], [28]. Since recording directly from many neurons simultaneously is impossible, measures have been taken to computationally visualize the response profiles of afferents more accurately. Population responses of rapidly-adapting (RA) afferents have shown sensitivity to their spatial organization, with significant differences between uniform and Gaussian distributions [29]. Other models have used metrics such as firing rate, spike timing, and response adaptation to assess the effects of skin elasticity, afferent density, and stimulus shape on simulated population responses with respect to the static and vibratory indentation of a wide range of stimuli [24], [26], [28], [30], [31], [32].

Aim 1. Differentiate unique contributions of neural afferent subtypes in encoding features of simulated food stimuli.

Abstract

Upon contact, the spike firing patterns of touch afferents encode object attributes such as force, vibration, and spatial geometry. Computational models in cutaneous skin have sought to emulate firing patterns of slowly and rapidly-adapting afferents. Herein, for the tongue, we develop biophysical versions of such models, which rely upon functions and parameters with physiological relevance, as opposed to stimulus features, and are extendable to a broad range of object interactions. The models are evaluated with mechanical inputs relevant to the oral processing of food, in particular, across stress ranges spanning material compliances and periodic vibrations emulating surface sliding. The results indicate the models

recapitulate spike firing patterns of human afferents innervating the tongue. Moreover, predicted patterns of spike firing, e.g., the mean and peak firing frequency, first spike latency, and number of spikes, compare favorably with neural recordings across force magnitudes, as do the number of spikes per cycle across a range of periodic amplitudes and frequencies. For extension into a population of afferents in oral mucosa, these single-unit models are a starting point for the further efforts to capture the encoding of higher-level perceptible attributes, e.g., compliance, geometry, surface roughness, and movement velocity.

Introduction

The mechanosensory capabilities of intra-oral structures, such as the tongue, play a fundamental role in enabling speech and the processing of food [33]. In contrast to cutaneous skin, where the encoding capacities of tactile afferents have been more comprehensively evaluated [9], [12], [34], [35], [36], prior studies are far less abundant in oral tissues [16], [19], [37], [38]. This is due, in part, to logistical challenges in obtaining electrophysiological recordings from afferents innervating the oral cavity, especially in humans. However, recent efforts in mice have begun to probe neural signaling properties via calcium imaging of cell bodies in trigeminal ganglion [19]. Moreover, solid mechanics measurements and models of the tongue are attempting to understand its nonlinear, anisotropic behaviors during speech and food processing [39], [40], [41].

In effort to understand the role of mouthfeel in the oral processing of food, computational models of the neural dynamics of spike firing may complement empirical observations. Despite prior biophysical [22], [23] and stimulus-dependent models in cutaneous skin [26], [32], [42], neural dynamics models have not been specialized to afferents of the oral cavity. Indeed, the tissue structure and neural innervation of the oral cavity may prove distinct from cutaneous skin. For instance, in one of few microneurography studies in human tongue, slowly (SA) and rapidly-adapting (RA) afferents are present, yet distinct from their cutaneous counterparts, with smaller receptive fields and lower detection thresholds [37]. As well, the presence of non-taste filiform papillae auxiliary structures in the tongue lead to patterns of innervation that contrast with those of hair follicles, intermediate ridges, and sweat ducts [12], [43]. Details regarding the

exact end-organ morphology of these afferents remain largely unknown, but likely differ from cutaneous Merkel cells, Ruffini endings, Meissner corpuscles, and Pacinian corpuscles [19], [33]. We do know, from calcium imaging studies at trigeminal ganglion, of at least five functional types of responders innervating mouse tongue, differentiated in terms of their force-response relations and adaptation profiles [33]. Two of these types, sustained and transient responders, behave somewhat similarly to slowly and rapidly-adapting afferents in cutaneous skin.

A better understanding of the role of mouthfeel in oral processing will require evaluating how a population of afferents captures perceptible attributes such as material compliance, spatial geometry, surface roughness, and movement velocity. Computational models of the neural dynamics of single units are prerequisite and slowly and rapidly-adapting afferents are the most direct link to prior observations in the tongue. As a basis for such efforts, we can look to numerous models of cutaneous skin afferents [22], [23], [26], [32], [42]. Many models have been stimulus dependent, in that they rely on stimulus displacement and multiple of its derivatives as inputs. Such dependence can require a model to be refit to new stimuli. In contrast, biophysical models have internal dynamics derived from physiologically measurable time constants and parameters.

This work develops biophysical models of mechanosensitive afferents in human tongue. Ramp-and-hold stimuli simulate forces during mastication and swallowing of foodstuffs. Periodic stimuli mimic behavior of food sliding over the tongue.

Methods

At the core of the computational model is a generator function, which converts tissue stress into mechanotransduction current, before a leaky integrate-and-fire function produces spike firing. Prior microneurography recordings from slowly and rapidly-adapting afferents in human, with forces induced by von Frey monofilaments are used to initially evaluate model produced instantaneous firing frequency. Using an experimental approach with two primary stimulus input modes, ramp-and-hold stress magnitudes over eleven levels (10-100 kPa), and periodic stimulus frequencies (5 to 300 Hz) and amplitudes (3.75 and 7.50

kPa to mimic 0 and -6 dB) are evaluated against data from the literature [34], [35], [44]. For the ramp-and-hold stimulus, output metrics include mean instantaneous firing frequency (IFF), peak IFF, first spike latency (timing of first spike after stimulus activation), and total number of spikes. For the periodic stimulus, the number of spikes per cycle is evaluated.

Biophysical Generator Function

In Fig. 1A, the generator function takes tissue stress as input and produces mechanotransduction current *I(t)*. Its mathematical form is adapted from a model specialized for slowly-adapting Merkel cell afferents in skin [22]. The model has been adapted to produce currents for both slowly and rapidly-adapting afferents, with its final parameters in Table 1.

The core distinction between the modeled generator functions for the SA and RA afferents lies in their individual mechanotransduction current components. In particular, the SA model includes three subcomponents of rapidly inactivating (RI), slowly inactivating (SI), and ultra slowly inactivating (USI) currents, which together determine the rate of current decay and adaptation to a stimulus. Each of these functions has time constant ($\tau_{RI},\ \tau_{SI},\ \tau_{USI}$) derived from the literature, and unique linear transformation coefficients *a, b,* and *c* that determine the relative contribution of each subcomponent to overall current. Moreover, the SI current includes a peak-to-steady state ratio (where $K_{SI_{Peak}} + K_{SI_{Steady}} = 1$). The $K_{SI_{Steady}}$ parameter is effectively 0 for the RI and USI terms [22]. In contrast to the SA generator function, the RA version uses only the RI component and *a* coefficient, as this afferent type exhibits a much more rapidly decaying current, and spike firing to held stimuli. Finally, the subcomponents of the model are convolved with a stress signal which is the weighted sum of the tissue stress and its rate of change, by parameters *g* and *h*. Mechanotransduction current *I(t)* is multiplied by -1 when below 0 to produce spikes during stimulus retraction. A leaky integrate-and-fire (LIF) model converts current *I(t)* to potential *u(t)*, producing a spike when potential is above a threshold of 30 mV before potential is reset [22], [23].

The biophysical generator function is distinct from typical stimulus-dependent models, Fig. 1B, where stimulus to tissue displacement (*x*) is used as input, and derivatives of velocity and acceleration are

separated into positive and negative components, assigned weights ($w_1 - w_6$), passed through a saturation filter using a separate I_0 parameter to generate mechanotransduction current. This type of model requires refitting of parameters to every new stimulus, which reduces its physiological relevance.

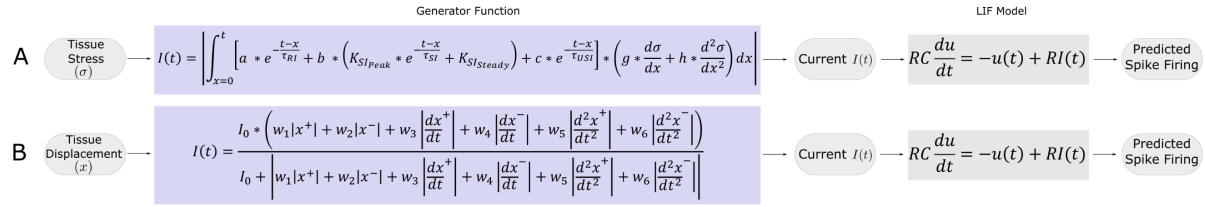

Fig. 1. Distinctions between biophysical and stimulus-based generator functions. (A) Biophysical function where tissue stress (σ) and its rate is convolved with current made up of the sum of three subcomponents of rapidly inactivating (RI), slowly inactivating (SI), and ultra slowly inactivating (USI) current, which determine the rate of adaptation to a stimulus. Each subcomponent has a corresponding time constant (τ_{RI}, τ_{SI}, τ_{USI}), and linear transformation coefficient (*a, b, c*). Additionally, the SI component includes a peak to steady-state ratio (where $K_{SI_{Peak}} + K_{SI_{Steady}} = 1$). (B) Typical stimulus-dependent function, where tissue displacement (*x*) is used as input, and its direct derivatives of velocity (first) and acceleration (second) are separated into positive and negative components, assigned weights ($w_1 - w_6$), passed through a saturation filter using a separate I_0 parameter to generate the mechanotransduction current. The current from either model passes through a leaky integrate-and-fire model which accumulates potential until a threshold is reached upon which a spike is fired and then potential is reset to zero.

Table 1.1. Parameters of Biophysical Generator function

	Parameter									
Afferent type	$\tau_{RI}(ms)$	$\tau_{SI}(ms)$	$\tau_{USI}(ms)$	***a***	***b***	***c***	$K_{SI\ Steady}$	$K_{SI\ Peak}$	***g***	***h***
Slowly-adapting	8	200	1744.6	0.74	2.75	0.07	0.13	0.87	0.4	1
Rapidly-adapting	2.5	0	0	35	0	0	0	0	0.4	1

Sensitivity Analysis

The model's range of output IFF was evaluated across a range of decay time constants (τ_{RI}) and linear transformation coefficients (*a* and *b)* which control the relative contributions of RI and SI currents. Fig. 2A (upper) modulates τ_{RI} of the simulated SA afferent at 1, 8, 30, and 100 ms for a ramp-and-hold stimulus. Fig. 2A (lower) modulates coefficient *b* at 2, 4, 8, and 16. Fig. 2B shows simulated RA afferent's response to a periodic stimulus at 10 Hz frequency and 3.75 kPa amplitude. Time constant τ_{RI} was tested at

1, 1.5, 2.0 and 2.5 ms (Fig. 3B, upper), and coefficient a at 10, 20, 30, and 40 (Fig. 2B, lower). The remaining model parameters were constant while τ_{RI} , a, and b were varied in the sensitivity analysis.

Model Fitting and Validation

The model's spike firing was evaluated, with stress input derived from a 5 mN von Frey monofilament and microneurography recordings from SA and RA afferents (Fig. 3) [37]. To approximate stress at a receptive field, the force was divided by the cross-sectional area of the monofilament. Its diameter is 0.05

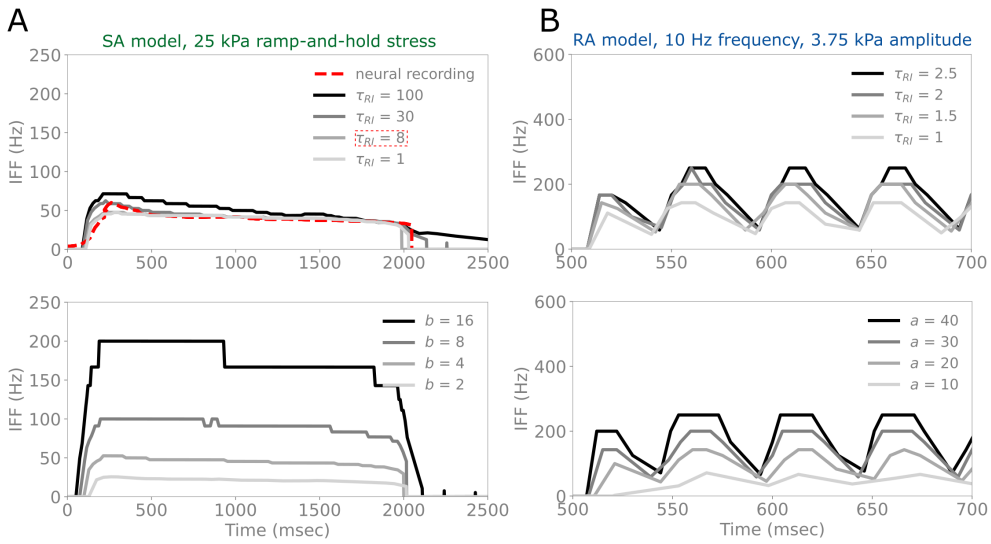

Fig. 1.2. Sensitivity of model spike firing with respect to parameter changes in the generator function. (A) SA afferent model's sensitivity to changes in the τ_{RI} time constant, which subtly affects the rate of decay in instantaneous firing frequency (IFF), and coefficient b, which affects the magnitude of IFF to a large degree. (B) RA afferent model's sensitivity to changes in the τ_{RI} time constant and coefficient a, during the first 200 msec of a periodic signal. The periodic signal is delivered atop a baseline stress level of 25 kPa, at a frequency of 10 Hz, and amplitude of 3.75 kPa, consistent with the periodic stimuli utilized in Fig. 3. As is observable, in panel B (top), a larger τ_{RI} time constant prolongs the decay in IFF and produces a higher peak IFF. In panel B (bottom), a larger coefficient a transformation coefficient increases the magnitude in IFF.

mm, producing a maximum stress of 25 kPa, when scaled down by a factor of 10e-2. Scaling was done to produce stress values of the same order of magnitude as in skin mechanics models of the human finger [45]. The model parameters, taken with biophysical assumptions in cutaneous skin [22], were manually tuned to match firing rates of afferents of the tongue (Fig. 3) with the final parameters listed in Table 1.

Experiments with Ramp-and-Hold, Periodic Stimuli

In Fig. 4, the model's response was evaluated over eleven stress magnitudes (10-100 kPa) [22], [45]. In Fig. 5, the model's response was evaluated over periodic frequencies (5-300 Hz*)* and amplitudes (3.75 kPa and 7.50 kPa to mimic amplitudes of 0 and -6 dB) [34], [35]. The periodic stimulus consisted of a 30 ms onset and offset duration to and from 25 kPa, with a periodic, sinusoidal stimulus from 500-1,500 ms.

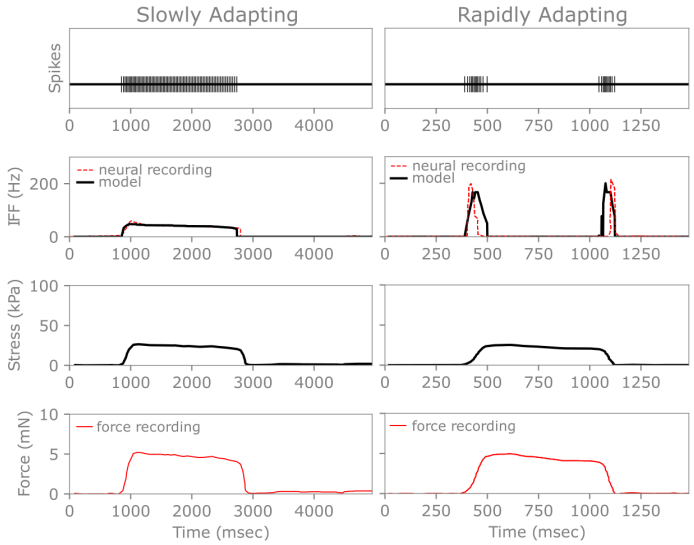

Fig. 1.3. Comparison of SA and RA model outputs to microneurography recordings in human tongue. (First row) Model produced spike firing for slowly (left column) and rapidly (right column) adapting afferents in response to ramp-and-hold stimulation by stress curve (third row) expected in tissue in response to an experimentally reported 5 mN von Frey monofilament (fourth row). (Second row) Instantaneous firing frequency (IFF) of the models replicates the actual recordings.

Results

Ramp-and-Hold Stress Magnitudes

Fig. 4A gives three exemplar traces of instantaneous firing frequency at stress levels 10, 25, and 80 kPa. Both models are sensitive to the level of input stress. The response of the simulated SA afferent displays sustained IFF over the course of the stimulus ramp at all three stresses. The response of the simulated RA afferent responds only at stimulus ramp and retraction, with the exception of a few spikes at 80 kPa due to slight force relaxation in this larger magnitude stimulus. These results are in line with general response

characteristics per afferent type (Fig. 3) and literature showing increased stress magnitude and rate increase IFF magnitude [44].

In Fig. 4B, the average IFF over the stimulus duration is shown across eleven magnitudes of stress. The response of the SA afferent model consistently exhibits a higher average firing rate than the RA model across stress levels, as it is not responding during the stimulus hold. Fig. 4C shows both models' peak IFF, first spike latency, and total number of spikes across stress levels. Fig. 4D compares normalized ranges (difference between minimum and maximum) for peak IFF, first spike latency, and number of spikes to prior work [44]. In particular, this study employed nine compliant, flat discs with stiffness from 0.21–7.79 mm/N, producing a large range of stress at the contact interface. Microneurography recordings in humans were collected from SA and RA afferents at force levels of 1, 2, 4 N. The SA and RA models' spike firing were compared to results obtained at 1 N across that paper's range of compliances. The SA and RA afferent models display similar behavior in terms of these metrics and their directionality, except for the peak IFF of the RA model. This may be due in part to differences in experimental conditions, as well as higher than expected sensitivity to change in stress by the modeled RA afferent. Relative to SA model, the RA model's peak firing rates are consistently higher across stress levels. The RA model saturates at 60 kPa, causing the peak IFF to remain at 500 Hz at higher stress levels until 100 kPa, which is not observed in actual neural data, and indicates an area yet to be addressed. First spike latency is consistently higher for the SA model, which is expected due to the RA afferent's sensitivity to change in stress. The SA model also produces more spikes, due to its sustained response to stimuli, relative to the RA's transient behavior.

Periodic Sinusoidal Frequencies and Amplitudes

In Fig. 5A, exemplar spike trains are shown for SA and RA models, in addition to their corresponding instantaneous firing frequency and stress traces, for a stimulus that ramps to 25 kPa, and includes a sinusoidal stress signal from 500 to 1,500 ms at 10 Hz. The two amplitudes exhibit distinct firing properties, with the 7.5 kPa case resulting in higher IFF during the periodic portion of the stimulus. This difference in firing is characterized by the number of spikes per cycle during the first 200 ms of the sinusoid

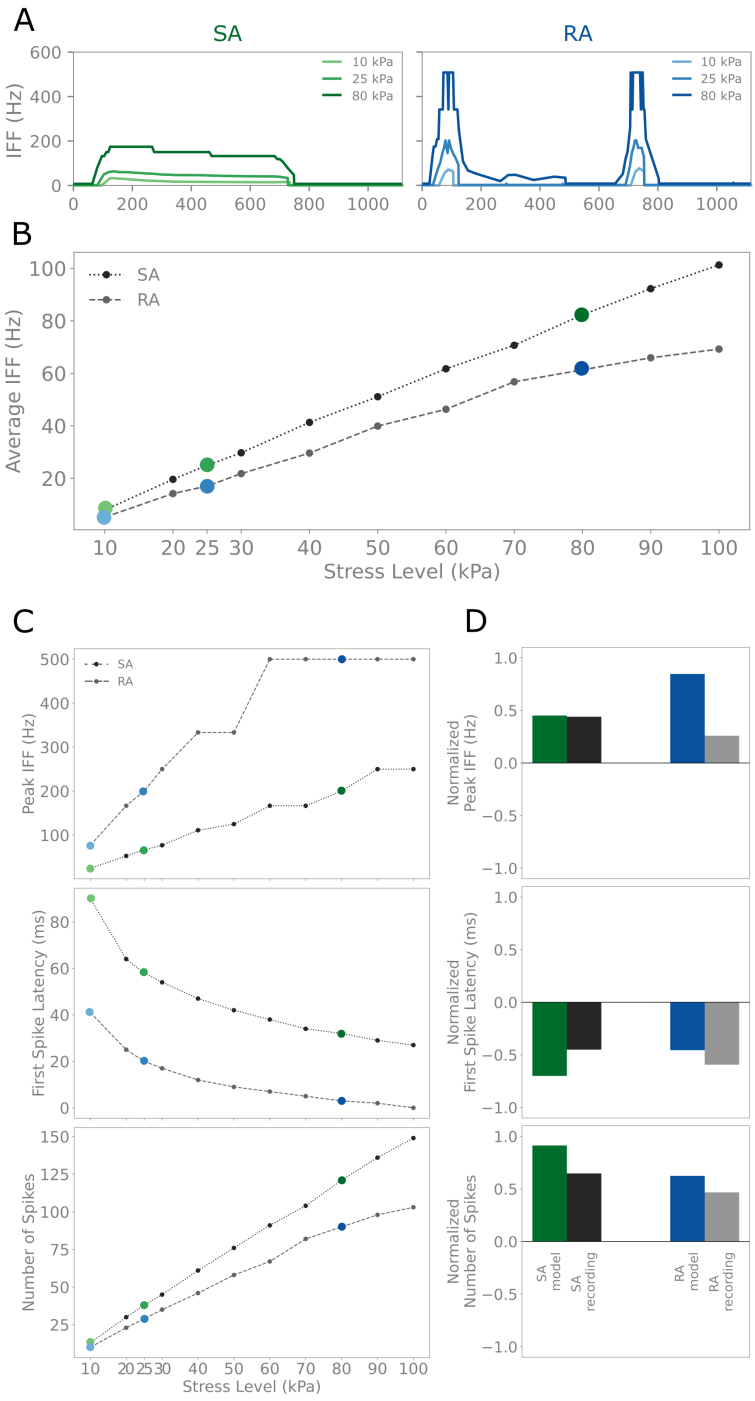

Fig. 1.4. Model responses across ramp-and-hold stress magnitudes. (A) Instantaneous firing frequency of slowly (green) and rapidly (blue) adapting models in response to ramp-and-hold stress magnitudes 10, 25, and 80 kPa. (B) Model derived average IFF per afferent type across all stress levels. Colored data points correspond to traces in panel A. (C) Peak IFF, first spike latency, and number of spikes across all stress levels. (D) Normalized relative differences of the summary statistics presented in panel C, captured across levels, in comparison to prior microneurography recordings to compliant stimuli which vary in effective force. The SA and RA afferent models display similar behavior in terms of these metrics and their directionality, except for peak IFF of the RA model, where there is a prominent difference with that of the neural recordings.

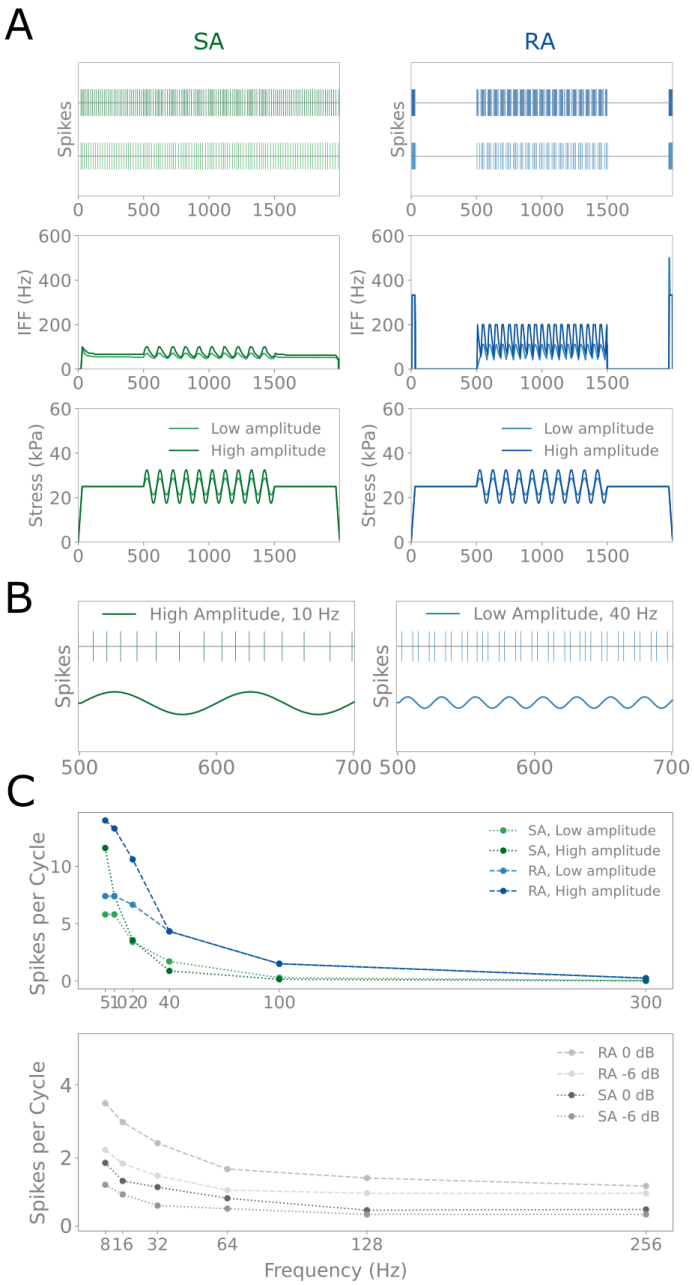

Fig. 1.5. Model responses across periodic frequencies and amplitudes. (A) Spikes and IFF produced by SA and RA models upon low (3.75 kPa) and high (7.50 kPa) amplitudes of periodic input. (B) Magnified view of spikes in relation to stress oscillations during the first 200 ms of the sinusoidal signal. The frequency of periodic stimulus has an inverse relationship with the total number of spikes produced in each of its cycles. (C) Total number of spikes per cycle produced (upper panel) by the model at two amplitudes and five frequencies in comparison to (lower panel) microneurography data at two amplitudes of 0 and -6 dB and six frequencies. The model and experimental amplitudes share the same power ratio, and are identical to those of panels A and B. The models' drop in the number of spikes per cycle with increase in frequency is consistent with the microneurography recordings. However, the number of spikes per cycle generated by the model are slightly higher. This is likely due to experimental stimulus differences in the absolute values of baseline stress and amplitudes of the periodic stimulus. More specifically, the microneurography data were collected with pure sinusoidal stimulation and not on top of the stress ramp into the skin as done with the model.

(Fig. 5B). The number of spikes per cycle are shown at 10 Hz with a high amplitude for the SA model, and 40 Hz with a low amplitude for the RA model. The number of spikes per cycle exhibit an inverse relationship with the frequency of the stimulus. Fig. 5C compares the number of spikes per cycle generated by the model for two amplitudes, and frequencies of 5, 10, 20, 40, 100, and 300 Hz with microneurography from SA and RA afferents in cutaneous skin [34] in response to sinusoidal skin displacements at similar frequencies and amplitude ratios. The models behave similarly in terms of spikes per cycle, with the RA model generally more sensitive across frequencies, and exhibiting the expected inverse relationship between frequency and number of spikes per cycle.

Discussion

The work in Aim 1 develops computational models for SA and RA mechanosensory afferents in human tongue. The models recapitulate the general spike firing patterns observed in microneurography recordings [37]. This work's focus on afferents of the oral cavity is distinguished from prior efforts in cutaneous skin [22], [23]. To simulate the range of forces occurring during mastication, as well as sliding behavior over a single afferent's receptive field, the model evaluates the encoding of stress magnitudes of ramp-and-hold stimuli and frequency/amplitude pairs of periodic stimuli. Such single-unit models are a building block towards population models as tied to the oral processing of food, likely to encode compliance, surface roughness, geometry, and movement velocity.

This effort centers upon biophysically relevant models, which differ from stimulus dependent models, in that they are fitted directly to the neurophysiology of mechanosensory afferents, and not the underlying stimulus. In particular, stimulus dependent computational models, such as those presented in [26], [42], employ assigned weights to tissue displacement and its derivatives to produce spike firing. Such dependence can require a model to be refit to new stimuli. Biophysical model parameters used herein are tuned from prior reports for slowly-adapting Merkel cell afferents in cutaneous skin, only quite minimally. Future work may be done to compare distinctions and implications in the parameters between body sites.

Prior efforts in the tongue have uncovered at least five functional types of afferents, including sustained and transient responders [16], [19], [37]. However, the end-organ morphology of these responders remains poorly understood, despite their behavioral similarities in spike firing responses with afferents in cutaneous skin [9], [12], [34], [36]. Microneurography in the human tongue poses significant logistical challenges, limiting the likelihood of a substantial increase in empirical data for various stimulation scenarios in the foreseeable future. Therefore, developing robust computational models of afferent populations may prove valuable to bridge gaps between neural mechanosensation and high-level perception in the oral cavity.

Areas for model improvement are first in its producing a higher than expected sensitivity to changes in stress for the RA afferent, particularly in terms of peak IFF. Second, the number of spikes per cycle evoked by the model for periodic stimuli are slightly higher than what has been reported [34]. More exhaustive parameter tuning methods such as grid search or Bayesian optimization might be employed in the future to address such discrepancies.

Aim 2: Develop an afferent population model to decode the geometry and diameter of simulated food stimuli.

Abstract

Sensory feedback from interactions with the tongue helps in encoding of the qualities of food during stages of oral processing. To augment physical mechanical measurements and perceptual studies in this domain, computational biophysical models of single mechanosensitive afferents have been developed to recapitulate spike firing patterns of human afferents innervating the tongue. However, the tongue is populated with thousands of single afferents, and from such population responses arise higher-level perceptible spatial attributes, e.g., stimulus diameter and geometry. Herein, we develop a population model of slowly-adapting (SA) and rapidly-adapting (RA) mechanosensitive afferents that vary in density and receptive field sizes, as informed by published human neurophysiological data from the tongue and the

glabrous skin of the hand. Configured in a population of 1,000 single afferent models (44% SA, 56% RA) over 50 by 25 mm cross-sectional area of the tongue, the model generates spike firing responses that can readily differentiate a set of 11 stimulus diameters from 0.05 to 20 mm, as well as blunt and curved geometric tips, while remaining insensitive to changes in stimulus position. Moreover, a Random Forest machine learning algorithm was employed to differentiate the stimuli from high-level spatial attributes, based on the total number of afferents recruited and total number of spikes elicited. Following efforts to mitigate risks of overfitting, using augmentation and cross-validation of training data, we achieved an 87.1% accuracy rate in classifying stimulus geometry, and a 0.55 mean-squared error (R^2 = 0.99) for diameter regression. Classification of the relative position of the stimulus yielded an approximately 50.5% mean accuracy rate, verifying the population model's invariance to stimulus position. This effort offers a foundational first step for building more complex mechanosensory models, affording the eventual encoding of stimulus compliance, surface roughness, and movement velocity, via their amalgamation with biomechanics of the human tongue.

Introduction

The sensory capabilities of the tongue are essential for encoding the perceptual qualities of food during oral processing, otherwise referred to as mouthfeel, through terms like 'firmness,' 'smoothness,' and 'thickness.' Numerous prior efforts have sought to study the encoding of such high-level attributes by evaluating the biomechanics of interactions of particular substances and the tongue. These approaches have sought to modulate tribological and rheological properties, e.g., textures of edible substances, to uncover whether they can be decoded by oral processing behaviors such as jaw movement and muscle activity, coupled with mastication forces, frequency, and duration [1], [2], [3], [4], [5], [6], [7], [8], [46]. Others, through solid mechanics measurements of the tongue, have tried to understand its nonlinear, anisotropic properties during speech and food processing [39], [40], [41]. Distinct from these biomechanical approaches, psychophysical methods, such as temporal dominance of sensation (TDS), have evaluated the dynamics of mouthfeel percepts such as 'crispiness,' 'brittleness,' and 'stickiness' during various stages of

chewing solid foods [5], [6]. These efforts report the subjective responses of human participants via numerical ratio scales at time intervals between 1 and 60 sec. [47].. Aside from these two distinct approaches – surface mechanics at the tongue and human perceptual responses – only a few efforts have sought to understand neural encoding mechanisms in between, i.e., input-output responses of peripheral neural afferents in signaling sensory and proprioceptive mouthfeel percepts.

A few empirical efforts have sought to measure peripheral neural responses underlying the tongue's sensory system, though at a rate far less than for cutaneous skin. Indeed, single neuron microneurography has been conducted in the lingual nerve innervating the human tongue [15], [16], [17], [37], while calcium imaging studies in mice have emerged to study populations of sensory cell bodies in the trigeminal ganglion [33]. While microneurography in humans may be easier to connect with perceptual responses, as opposed to animal models, recording directly from many afferents simultaneously is impossible, as attaining neural recordings in humans are often risky and tedious, due to tongue innervating nerves near the neck and head. From the latter studies, we have begun to learn of functional similarities to slowly and rapidly-adapting afferent subtypes of cutaneous skin, though with distinctions in input-output response properties, receptive field sizes, and the ratio of slowly to rapidly-adapting units [19], [33], [43]. However, such studies are limited to animal models, where it is more challenging to conduct perceptual experiments and have evolved distinct dietary characteristics. For these reasons, computational models offer a practical approach.

In **Aim 1**, we developed and validated single unit, biophysical models of mechanosensitive afferents for the human tongue, which encode ramp-and-hold forces to simulate mastication and swallowing foodstuffs, and periodic movements to emulate food sliding over the tongue. However, a model of a population of afferents is sought as the tongue is populated with thousands of single afferents, and from such population responses arise perceptible spatial attributes, e.g., stimulus diameter, geometry, and motion of food interactions. Indeed, prior efforts in cutaneous skin have produced population responses, via top-down definition of metrics tied to overall firing magnitude and rate, between afferent spike timing. Such models have sought to evaluate a simulated population's response given distinct afferent densities, spatial

arrangements, stimulus geometries, and skin elasticities [26], [28], [30], [31], [32], [48]. For instance, Guclu and Bolanowski showed that spatial organization of rapidly-adapting afferents affect their population responses, with significant differences reported between uniform and Gaussian distributions [29]. In general, the principle of reciprocal interpretation [27], [28] – which posits that the collective response of an afferent population can be inferred from the response of individual, or a small subset of afferents– provides the basis for computational approximation of afferent population responses. That said, all of the prior efforts have been designed and validated for tactile afferents in cutaneous skin. Moreover, in contrast with these top down approaches – where metrics such as firing rate and first spike latency are defined a priori – many machine learning and statistical inference efforts have used a bottom up approach to learn stimulus metrics from population response profiles [49], [50], [51], [52], [53], [54], [55], [56], [57]. For instance, advanced techniques coupled with information-theoretic analysis [58], [59] have shown that stimulus size, vibrational frequency, ramp length, and ramp amplitude can be decoded by the activity of afferent populations, varying in density, in glabrous skin of hand [54].

Herein, to generate a population response to decode stimulus geometry and diameter, we develop a computational model in the context of single unit models, receptive field sizes, and ratios between SA and RA afferents attuned to the tongue. We seek to identify the optimal population density to complete these tasks, while remaining insensitive to changes in stimulus position over a 2D cross-sectional area representing the tongue. Moreover, in addition to the traditional statistical evaluation of population responses by metrics of total spikes and number of afferents recruited, a machine learning algorithm is employed to classify a presented stimulus diameter and geometry. Overall, this effort seeks to establish a foundational first step for building more complex mechanosensory models, affording the eventual encoding of stimulus compliance, surface roughness, and movement velocity, via their amalgamation with biomechanics of the human tongue.

Methods

The single unit models developed for slowly-adapting and rapidly-adapting afferents in **Aim 1** were adapted for response to stimuli that were not directly above their receptive field. The core of the biophysical model for neural dynamics, i.e., the generator function and leaky-integrate-and-fire model (LIF), as well as their parameters, were not modified. By employing this new spatially sensitive single-unit model, a map was developed on a 50 x 25 mm cross-sectional area of a simulated human tongue. The SA and RA afferents were distributed according to a uniform probability density function, with varying total afferent densities and receptive field sizes. The ratio between SA and RA afferents remained constant at 0.786 (44% SA, 56% RA), while stimuli of varying tip geometry (curved/blunt), diameter, and relative position were indented onto the population. The total number of recruited afferents per subtype, and the total number of spikes per subtype elicited by the stimulation were used as fundamental population metrics to evaluate whether geometry, diameter, and position can be differentiated. A predictive machine learning model (Random Forest) was used to classify stimulus spatial elements according to their spike firing metrics at the population level.

Computational Experiment I. Spatial Model of Single-unit Afferents

Assuming reciprocal interpretation, a spatial response profile was built for a blunt and curved stimulus, as they were indented normally at increments of 0.2 mm over the receptive field of a single SA or RA afferent, as shown in Fig. 2.1. The response profile was designed based on neural data derived from [60], [61], where the normalized response of an afferent was reported to be approximately 20% of its absolute value in the center of a blunt stimulus, with respect to its edges (Fig 2.1A). As an approximation for a curved stimulus, it was assumed that this response profile is inverted, and that the normalized response of a single afferent will be 20% of its absolute value at the edges of the stimulus contact area (Fig 2.1B).

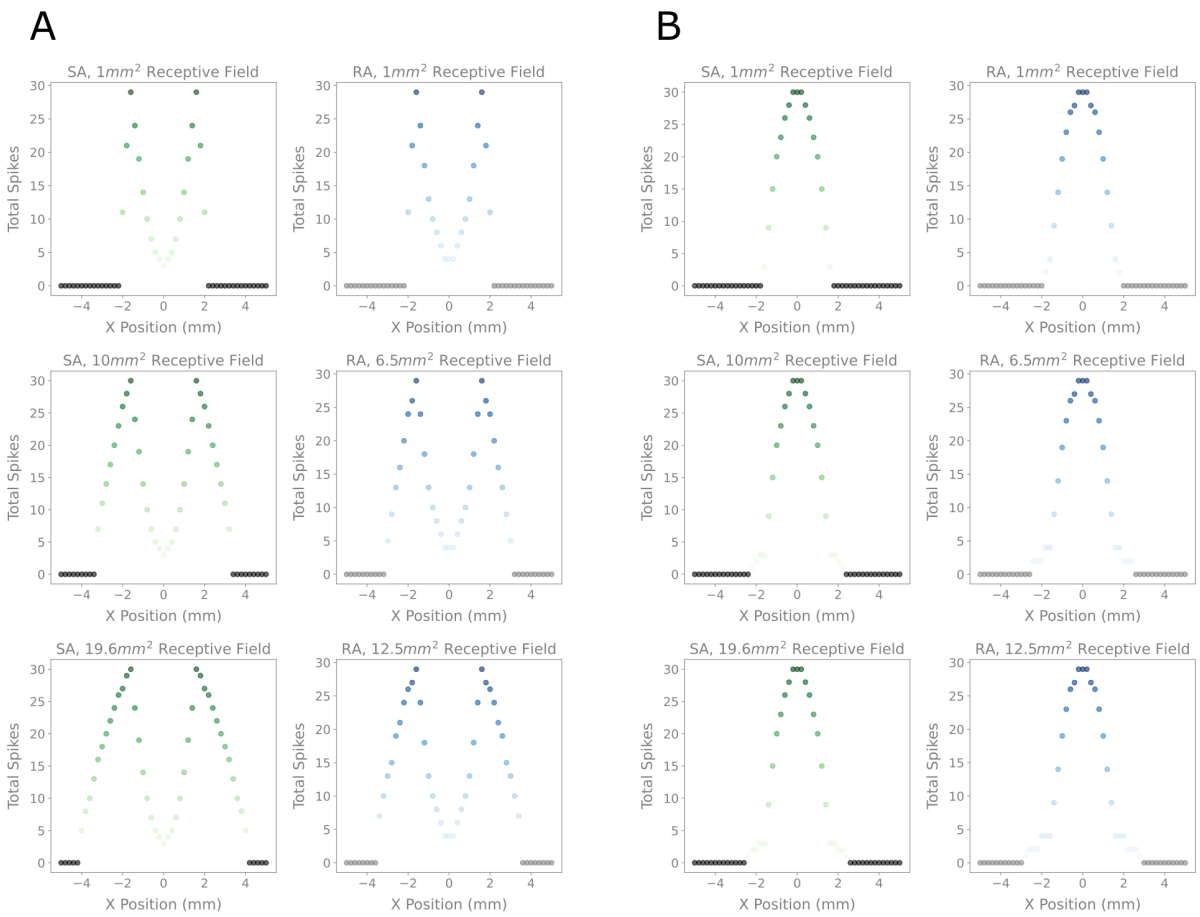

Fig. 2.1. Number of total spikes elicited by a blunt and curved stimulus, across receptive field sizes. A stimulus is normally indented at 50 distinct spatial locations, moving from -5 to 5 mm at a resolution of 0.2 mm. The stimulus was 3.17 mm in diameter for all experiments. The number of spikes are recorded in response to a blunt (A) and curved (B) tip stimulus, as the receptive field sizes of the SA (1 to 19.6 mm^2) and RA (1 to 12.5 mm^2) afferents are modulated. The blunt stimulus elicits a response which produces maximal stress at the edges of the stimulus, whereas the curved stimulus produces the maximum at the center of the stimulus.

The receptive field sizes for the SA (1, 10, 19.6 mm^2) and RA (1, 6.5, 12.5 mm^2) afferent subtypes were derived from [62], where 10 and 6.5 mm^2 were chosen as median values of what was reported as the smallest and largest receptive field size for slowly-adapting and rapidly-adapting afferents in human glabrous skin of the hand (rounded up to the nearest whole number), respectively. A single unit will produce a firing response depending on its Euclidean distance from the center (curved), or edge (blunt) of the stimulus, using the same biophysical computational model developed and validated in **Aim 1**. The piecewise functions governing the absolute value of normal stress, with respect to its distance from the

center of an afferent's receptive field are shown in Eq. 1 (blunt stimulus) and Eq. 2 (curved stimulus). Where σ is normal stress, (x_s, y_s) are the position of the stimulus center, (x_k, y_k) are the position of the receptive field center, r_s is the radius of the stimulus, r_{RF} is the radius of the receptive field, and ε is the computational tolerance.

$$\sigma = \begin{cases} \sigma & if\ |D - r_s^2| \le \varepsilon \\ (0.8 * \left(\frac{D}{r_s^2}\right) + 0.2)\sigma & if\ D \le r_s^2 \\ \left(\frac{-0.8 * D + (r_s + r_{RF})^2 - 0.2 * r_s^2}{(r_s + r_{RF})^2 - r_s^2}\right)\sigma & if\ r_s^2 < D \le (r_s + r_{RF})^2 \\ 0 & if\ D > (r_s + r_{RF})^2 \end{cases}$$

$$where\ D = (x_k - x_s)^2 + (y_k - y_s)^2$$

$$\varepsilon = 10^{-3}\ mm$$

(Eq. 1)

$$\sigma = \begin{cases} \left(1 - 0.8\frac{D}{r_s^2}\right)\sigma & if\ D \le r_s^2 \\ \left(-0.2\frac{(D - r_s^2)}{(r_s + r_{RF})^2 - r_s^2} + 0.2\right)\sigma & if\ r_s^2 < D \le (r_s + r_{RF})^2 \\ 0 & if\ D > (r_s + r_{RF})^2 \end{cases}$$

$$where\ D = (x_k - x_s)^2 + (y_k - y_s)^2$$

(Eq. 2)

Computational Experiment II. Population Model of Afferents in Human Tongue

A population model of afferents was simulated by distributing the single units tuned in Computational Experiment I, over a 50 x 25 mm cross-section of a hypothetical, two-dimensional human tongue. This model receives as input, a single stress trace and stimulus metrics, e.g., diameter, geometry, and calculates the normal stress over time on the receptive field of each afferent in the population, according to its receptive field center's distance from the stimulus edge, or center for curved stimuli. The normal stress traces of each afferent are then received by the generator function and leaky-integrate-and-fire model,

developed in **Aim 1**, subsequently producing spike times, based on the afferent subtype, e.g. SA or RA.

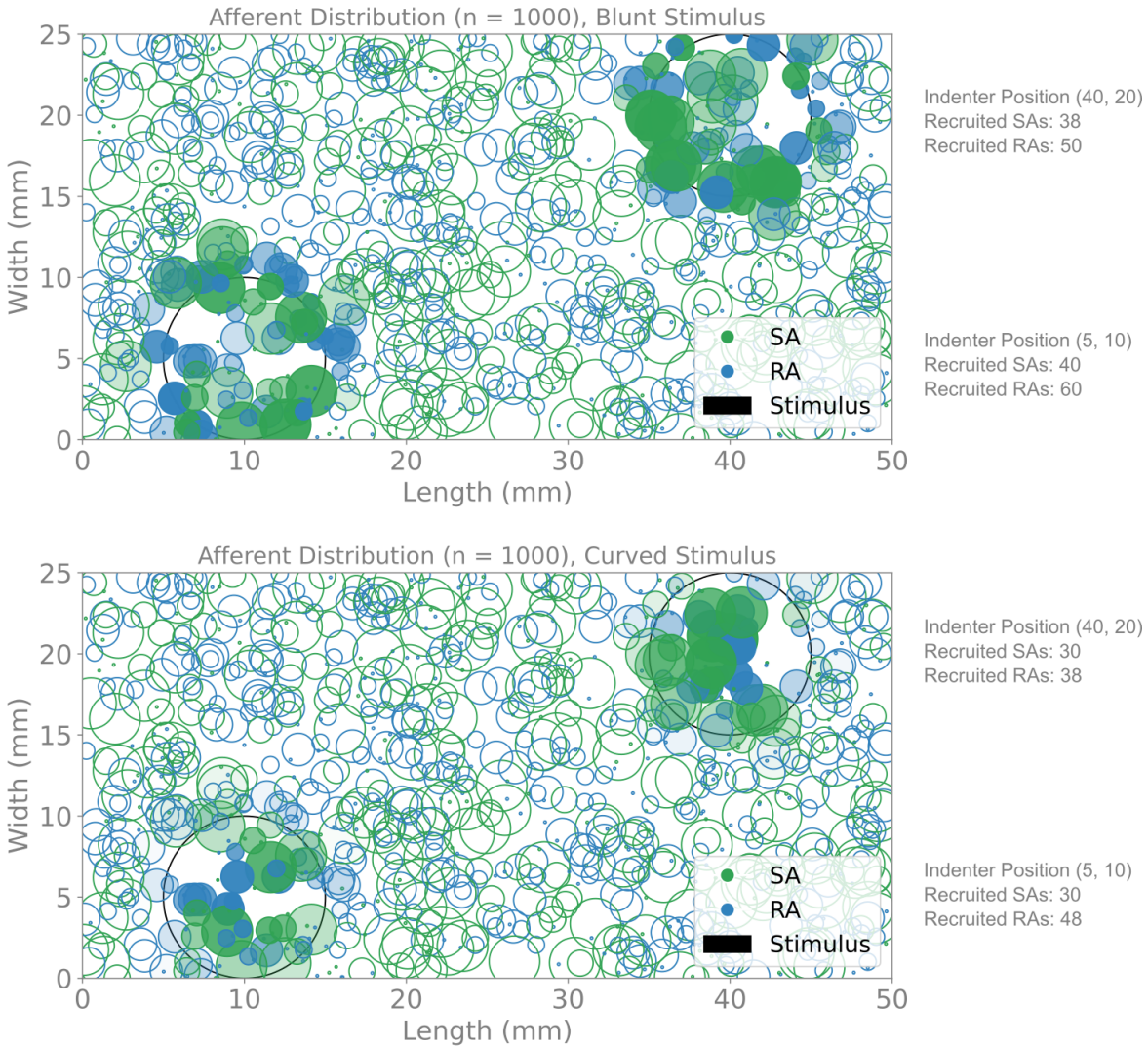

Fig. 2.2. Population model simulation of blunt (top) and curved (bottom) stimulus. A sample simulation of the population model of afferents over a 25 x 50 mm cross-section of the tongue is shown, for a 10 mm diameter stimulus. Afferent locations were produced through a uniform distribution for both stimulus types, as well as a uniform distribution for each afferent's receptive field size. The viable options for SA receptive field sizes were 1, 10, 19.6 mm^2, and 1, 6.5, 12.5 mm^2 for RA afferents. The opacity of the afferents' receptive fields are determined by their response intensity, dependent on their Euclidean distance from the edge for the blunt stimulus, and center for the curved stimulus, respectively. This simulation was run with 1000 total afferents, with 44% SA and 56% RA. The distribution of afferent subtypes remains constant throughout this effort, with a 44% probability of being SA, and 56% probability of being an RA afferent.

Spike times and afferent recruitment were aggregated across the population to produce outputs of total number of spikes, and total number of afferents recruited, per subtype. The afferent locations were

distributed using a uniform probability density function, with a 44% probability of the subtype being SA, and a 56% probability of being RA, as reported for the glabrous skin of the human hand [62]. The total number of afferents could be modulated as desired, but the distribution between subtypes were kept constant in this effort. The afferent receptive field sizes were also determined from a uniform probability density function A sample simulation for a blunt and curved stimulus is shown in Fig. 2.2., with a total of 1000 afferents (n = 1000) across both subtypes, for a 10 mm diameter stimulus at two distinct positions. A darker opacity for a particular afferent's receptive field signals a higher firing intensity, based its distance from the stimulus center, dependent on its geometry.

The total number of afferents in the population were chosen by optimizing model outputs for minimal relative variance in the two fundamental population metrics of total number of spikes and total number of afferents recruited per subtype, as the spatial position of the stimuli were modulated. In Fig. 2.3., population responses were calculated and recorded for the SA and RA afferents separately, at four (x, y) mm positions of (10, 5), (40, 5), (10, 20), and (40, 20) mm, as the total number of afferents were modulated to seven quantities varying from 25 to 5000. A 10 mm diameter, blunt stimulus was used for this simulation. While it can be gleaned from Fig. 2.3 that the relative variance between the population metrics decreases significantly after 500 afferents, a more precise quantitative measure of variance is presented in Fig. 2.4. via the mean coefficient of variation for the total number of spikes and total afferents recruited, over the aforementioned four positions. The goal from this section of the work was to build a model that is spatially invariant. In particular, a population model that is not extremely sensitive to the relative position of the stimulus, which was achieved by using 1000 total afferents, with no significant reduction in the coefficient of variation above this point.

Computational Experiments III. Differentiation of Stimulus Geometry and Diameter

Population responses were simulated by the computational model across 20 (x, y) mm positions over the tongue cross-section, with possible values for x being 10, 20, 25, 30, 40 mm, and possible values for y being 5, 10, 15, 20 mm. The stimulus geometry was modulated between a curved and blunt tip, each

designed to produce distinctive stress distribution profiles at the contact interface. For both stimulus geometries, simulations were run across 10 diameters ranging from 0.05 to 20 mm. A diameter of 3.17 mm was also tested in addition to the others, in an effort to relate stimulus sizes to prior literature [31]. The total number spikes produced by every afferent that was activated in the population during the stimulus indentation (onset, hold, offset), and the total number of afferents recruited – an afferent was considered recruited if it produces at least one spike over the experiment duration – were compared across both stimulus geometries, and all 11 diameters. Pairwise t-tests were performed for both population metrics across all diameters, to test statistical significance of the differences in mean between the curved and blunt stimulus. For the 3.17 mm diameter stimulus, the temporal accumulation of these population metrics was collected as well across the 20 spatial positions, in an effort to visualize whether the curved and blunt stimulus are differentiable before the terminal state of the stimulus.

Computational Experiment IV. Prediction of Stimulus Geometry, Position, and Diameter using Population Response Metrics

A Random Forest algorithm, with 5-fold cross-validation, and a 70/30 train-test split of data was used to make predictions of stimulus geometry, position, and diameter. The four features used for training and fitting the Random Forest model were the total number of spikes for SA, total number of spikes for RA, total number of recruited SA afferents, and total number of recruited RA afferents, over the entirety of the population. 5-fold cross validation were performed to mitigate the risk of overfitting.

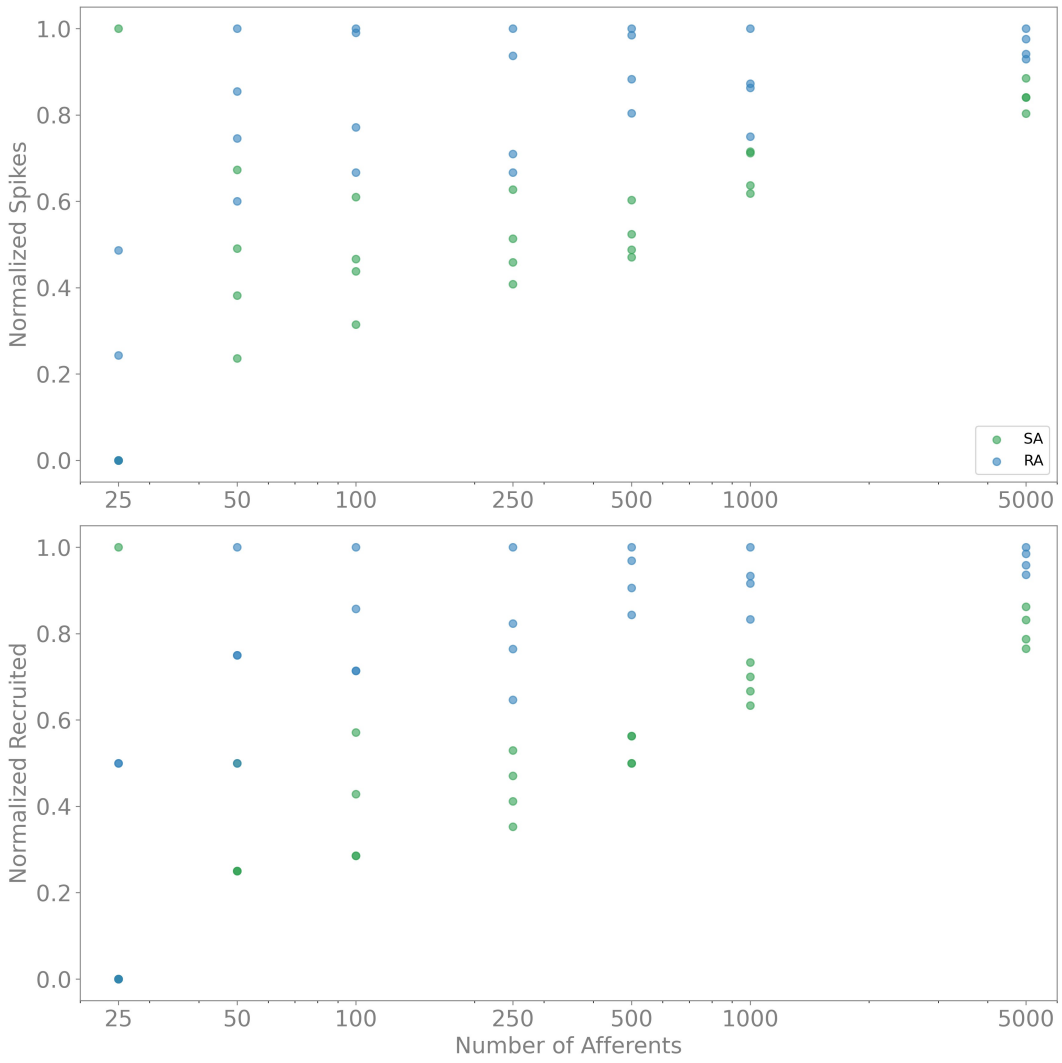

Fig. 2.3. Normalized population responses of SA and RA afferents as total afferent density increases. Normalized population responses for total number of spikes (top) and total afferents recruited (bottom) are shown as the afferent density is increased from 25 to 5000. This simulation was run at four distinct positions on the tongue cross-section, characterized by the (x, y) mm pairs of (10, 5), (40, 5), (10, 20), and (40, 20) mm. The relative variance between the responses for SA and RA decreases as the afferent density increases. This decrease in variance is especially noticeable above 500 afferents. The stimulus had a blunt tip, and a diameter of 10 mm.

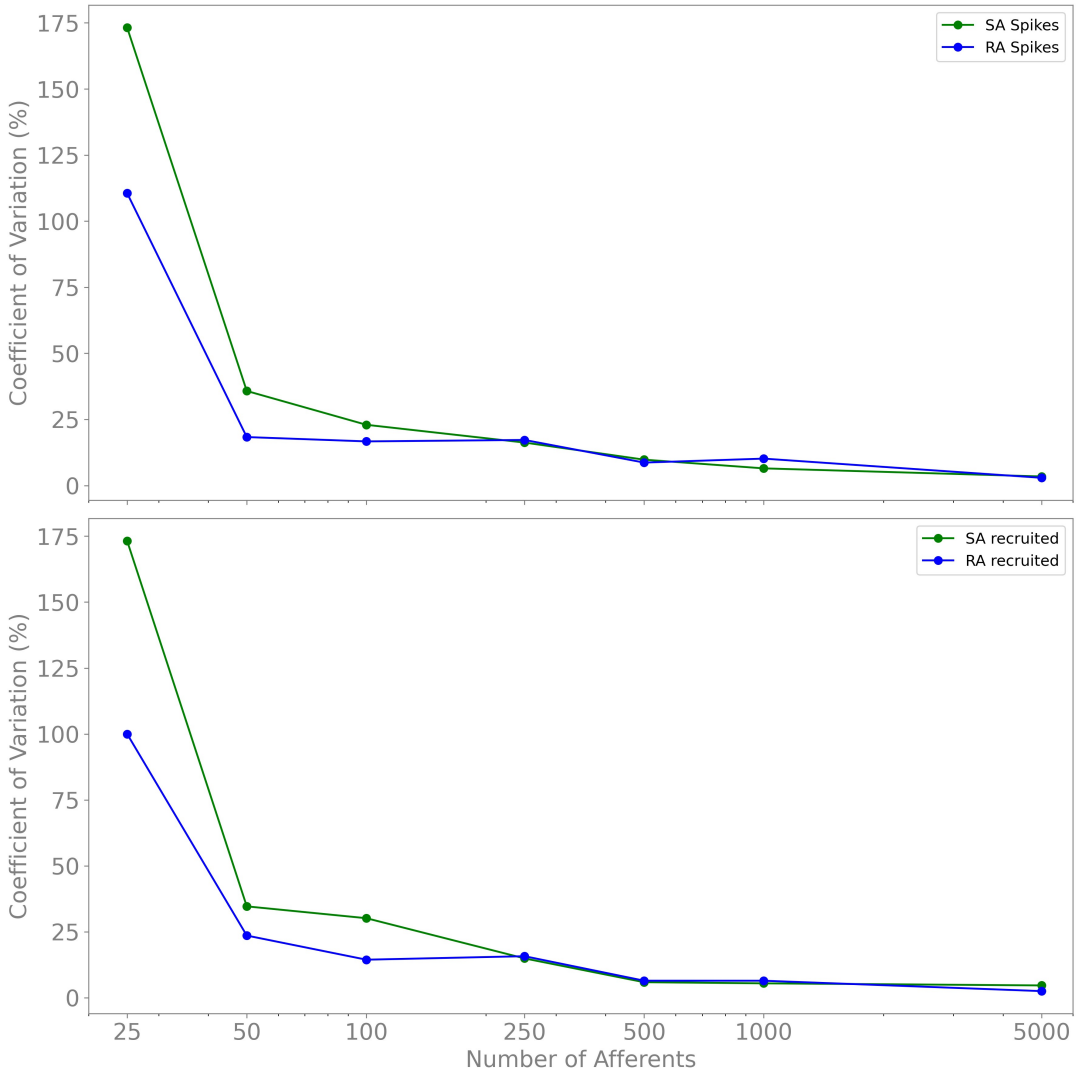

Fig. 2.4. Coefficient of variation for population metrics across afferent densities. Building upon Fig. 2.3., the mean coefficient of variation is shown for population metrics of total spikes and total number of afferents recruited, as a more precise measure of relative variance as afferent density increases. The population model is stable at 1000 afferents, which was chosen to run further experiments. The stimulus used was blunt, with a 10 *mm* diameter, indented at 4 distinct positions, as in Fig. 2.3.

Results

Computational Experiment III. Differentiation of Stimulus Geometry and Diameter

An in-depth analysis of the 3.17 mm diameter stimulus is presented in Fig. 2.5 and Fig. 2.6 for 1000 total afferents. In Fig. 2.5, the distribution of the population metrics is shown for a curved and blunt

stimulus across 20 positions, with separate boxplots for the SA and RA subtypes. The stimulus geometry is reliably differentiated by the model for both afferent subtypes at the terminal state of the experiment, with slightly higher median values elicited by the RA afferent. This can be attributed to the higher density of RA afferents in the population, as compared to SA. In Fig. 2.6, the accumulation of median population metrics is shown over time, for the curved and blunt stimuli. The shaded regions indicate the inter-quartile range (IQR). Once again, stimulus geometry is reliably differentiable, over the entire duration of the experiment with the blunt stimulus producing a higher number of spikes and recruited afferents overall.

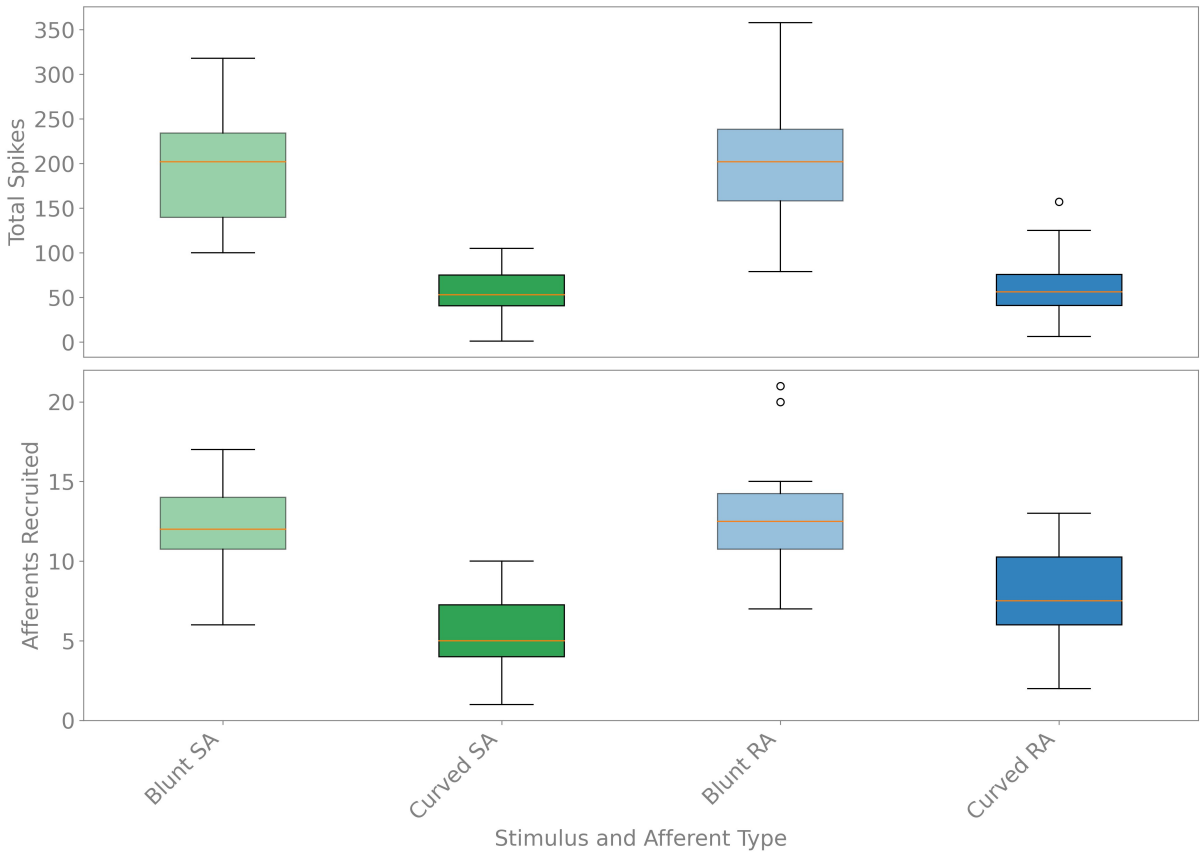

Fig. 2.5. Comparison of population responses for blunt and curved stimuli. (A) Population response distributions across 20 distinct spatial points of stimulation for a curved and blunt stimulus, of a 3.17 mm diameter. The stimulus type is reliably differentiated across both population metrics of total spikes (top) and total afferents recruited (bottom). The median RA response is slightly higher than the median SA response for both metrics.

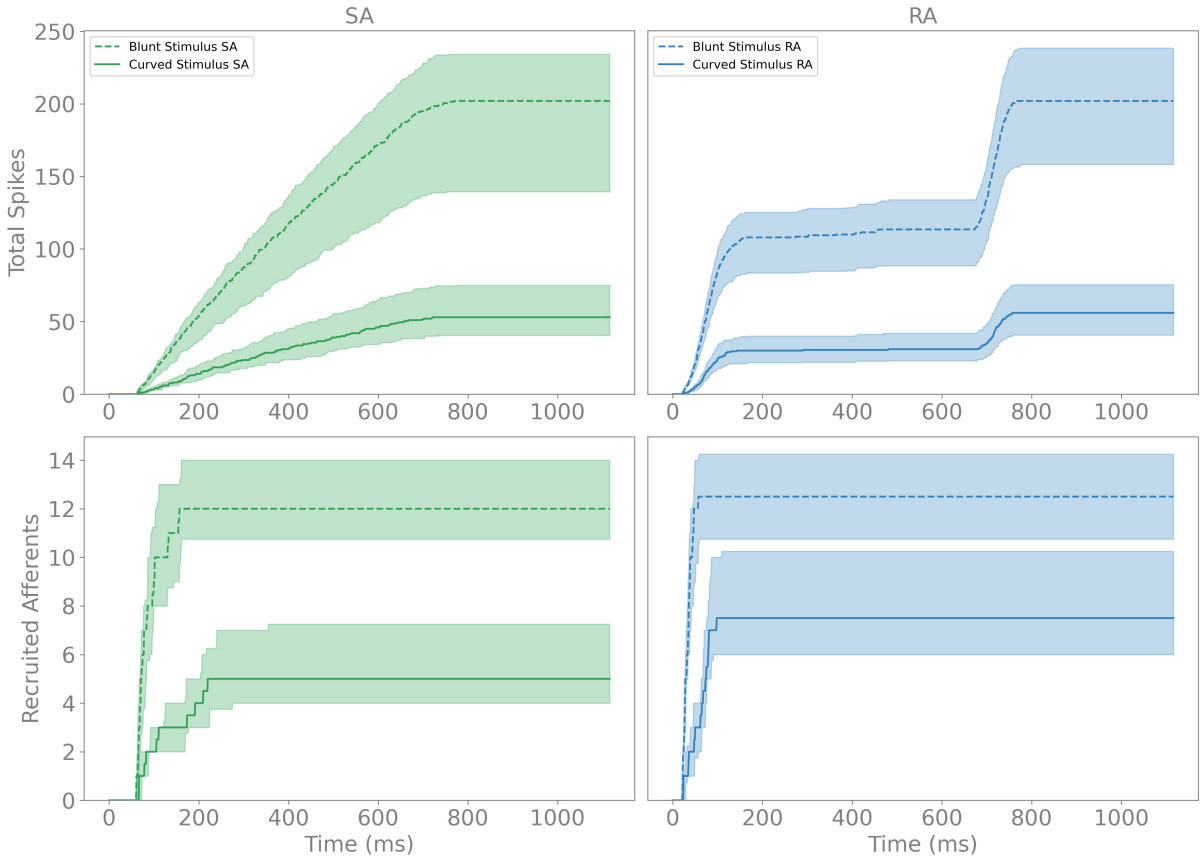

Fig. 2.6. Temporal accumulation of median population responses. (A) Median population responses over time, as the 3.17 mm diameter stimulus is indented, across 20 distinct points on the tongue cross-section. Blunt and curved stimuli are reliably differentiable over time for both population metrics, with the blunt stimulus consistently eliciting a higher rate of accumulation. Shaded regions indicate the inter-quartile range (IQR) for each metric.

In Fig. 2.7, a more comprehensive experiment is shown across 11 stimulus diameters, ranging from 0.05 to 20 mm for 1000 afferents. Each stimulus was indented at the same 20 positions (n = 20) as the 3.17 mm stimulus. Error bars indicate standard deviation. Blunt and curved stimuli are robustly differentiable across a wide range of diameters, with pairwise t-tests performed at each diameter/population metric pair to show statistical significance. These results are shown in Table 2.1, with highly significant differences in mean for every case (p-value < 0.01), except for the total number of recruited RA afferents for the 20 mm stimulus (p = 0.0694). Within a stimulus geometry type, the diameters are highly differentiable for values larger than 1.0 mm, but only slightly different for diameters 0.5 mm and smaller.

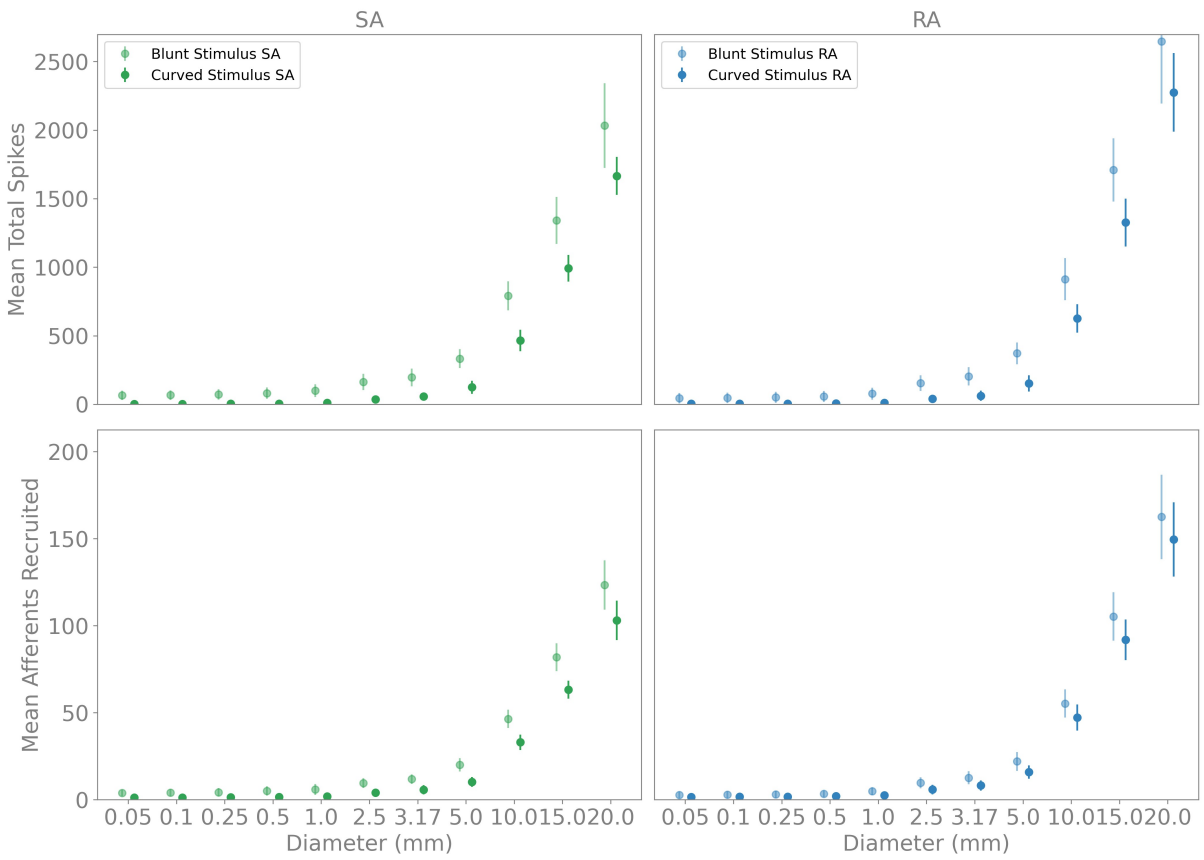

Fig. 2.7. Population responses for blunt and curved stimuli across stimulus diameters. As a comprehensive experiment to compare blunt and curved stimuli, the stimulus diameter was modulated from 0.05 to 20 *mm*, at 20 distinct spatial points, while population responses were recorded. The data for the 3.17 *mm* stimulus were included here to showcase a direct comparison to other stimulus diameters. Blunt and curved stimuli are robustly differentiable across a wide range of diameters, with pairwise t-tests performed at each diameter to show statistical significance. These results are shown in Table 2.1, with highly significant differences in mean.

Computational Experiment IV. Prediction of Stimulus Geometry, Position, and Diameter

In Fig. 2.8, Random Forest classification was performed, using 5-fold cross-validation to mitigate the risk of overfitting, was performed for classifying stimulus geometry (top left), and relative position (X dimension top right, Y dimension bottom left). The data included population responses for curved and blunt stimuli, at 20 positions, and at all diameters used in Fig. 2.7. The model can reliably classify geometry (mean accuracy 90.85%), but below chance (50% accuracy) for most x (mean accuracy 40.9%) and y positions (mean accuracy 43.1%).

Table 2.1. Statistical significance of differences between curved and blunt stimuli

Diameter (mm)	Metric	t-statistic	p-value
0.05	SA Total Spikes	8.2153	< 0.0001
0.05	RA Total Spikes	4.7524	0.0001
0.05	SA Total Afferents Recruited	6.1677	< 0.0001
0.05	RA Total Afferents Recruited	2.0811	0.0444
0.1	SA Total Spikes	8.2341	< 0.0001
0.1	RA Total Spikes	4.8281	0.0001
0.1	SA Total Afferents Recruited	6.0184	< 0.0001
0.1	RA Total Afferents Recruited	2.0582	0.0468
0.25	SA Total Spikes	7.9718	< 0.0001
0.25	RA Total Spikes	5.078	0.0001
0.25	SA Total Afferents Recruited	5.4341	< 0.0001
0.25	RA Total Afferents Recruited	2.2026	0.0339
0.5	SA Total Spikes	8.208	< 0.0001
0.5	RA Total Spikes	5.5864	< 0.0001
0.5	SA Total Afferents Recruited	6.0885	< 0.0001
0.5	RA Total Afferents Recruited	2.5001	0.017
1	SA Total Spikes	8.2967	< 0.0001
1	RA Total Spikes	6.7761	< 0.0001
1	SA Total Afferents Recruited	5.5968	< 0.0001
1	RA Total Afferents Recruited	3.6076	0.0009
2.5	SA Total Spikes	8.8716	< 0.0001
2.5	RA Total Spikes	7.9534	< 0.0001
2.5	SA Total Afferents Recruited	7.6538	< 0.0001
2.5	RA Total Afferents Recruited	4.3877	0.0001
3.17	SA Total Spikes	8.9339	< 0.0001
3.17	RA Total Spikes	8.363	< 0.0001
3.17	SA Total Afferents Recruited	7.8903	< 0.0001
3.17	RA Total Afferents Recruited	4.4082	0.0001
5	SA Total Spikes	11.2133	< 0.0001
5	RA Total Spikes	9.8932	< 0.0001
5	SA Total Afferents Recruited	9.7146	< 0.0001
5	RA Total Afferents Recruited	4.3703	0.0001
10	SA Total Spikes	11.0785	< 0.0001
10	RA Total Spikes	6.9241	< 0.0001
10	SA Total Afferents Recruited	9.373	< 0.0001
10	RA Total Afferents Recruited	3.4301	0.0015
15	SA Total Spikes	7.9064	< 0.0001
15	RA Total Spikes	5.9398	< 0.0001
15	SA Total Afferents Recruited	9.0166	< 0.0001
15	RA Total Afferents Recruited	3.4381	0.0015
20	SA Total Spikes	4.8634	< 0.0001
20	RA Total Spikes	3.1053	0.004
20	SA Total Afferents Recruited	5.1995	< 0.0001
20	RA Total Afferents Recruited	1.8698	0.0694

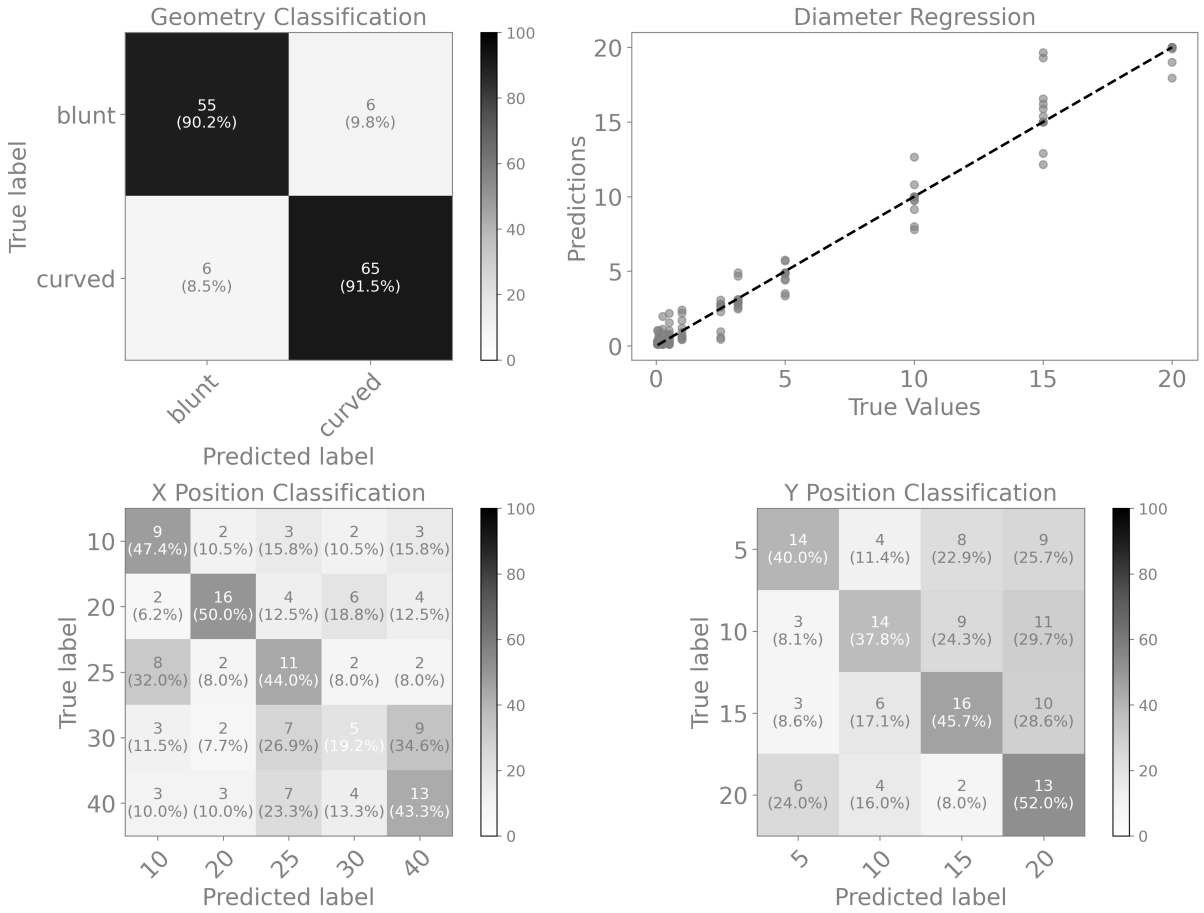

Fig. 2.8. Prediction of stimulus geometry, relative position, and diameter using a Random Forest algorithm. Random Forest classification, using 5-fold cross-validation to mitigate the risk of overfitting, was performed for classifying stimulus geometry (top left), diameter (top right), and relative position (X dimension bottom left, Y dimension bottom right). The data included population responses for curved and blunt stimuli, at 20 positions, and at all diameters used in Fig. 2.7. The model can reliably classify geometry (mean accuracy 90.85%), but below chance (50% accuracy) for most x (mean accuracy 40.9%) and y (mean accuracy 43.1%) positions. This indicates the model is invariant in response to spatial modulation of the stimulus, meaning the afferent density is sufficient at 1000 afferents. Using the same overfitting prevention techniques, Random Forest regression was implemented for diameter prediction. This yielded an MSE of 0.92, and an R^2 score of 0.98, indicating robust stimulus diameter prediction.

This indicates the model is invariant in response to spatial modulation of the stimulus, meaning the afferent density is sufficient at 1000 afferents. Using the same overfitting prevention techniques, Random Forest regression was implemented for diameter prediction. This yielded a mean-squared error of 0.92 mm^2, and an R^2 score of 0.98, indicating robust stimulus diameter prediction.

Discussion

This work develops a biophysical afferent population model to encode the geometry and diameter, of simulated food stimuli. The model focuses on how a population of slowly-adapting and rapidly-adapting mechanosensory afferents, varying in density and receptive field sizes, can differentiate stimulus geometry and diameter, as they are indented at distinct positions. This effort extends beyond single-unit models (**Aim 1)**, to capture emergent population-level behaviors, essential for understanding the neural encoding of high-level perceptible attributes.

Population response metrics, such as total number of spikes and recruited afferents, were used as the fundamental method to differentiate blunt and curved stimuli across a range of 11 diameters, and at 20 distinct positions. The results, confirmed through statistical analyses and machine learning techniques, indicate that these metrics can indeed encode the shape and size of food stimuli, although is model's efficacy in differentiating spatial positioning is less robust, performing only slightly above chance (50% accuracy). However, this insensitivity is positive in the sense that a human tongue will likely perform in the same way, given its high afferent density. For instance, two stimuli of identical force and diameter will elicit identical perceptual cues on the tongue, albeit at two distinct points of contact. In retrospect, in predicting stimulus position, an improved method would be to train a regression model on the L2-norm of (x, y) mm pairs, using a point of reference, such as the center of the tongue cross section, as the origin. This would combine both dimensions into a single value, rather than requiring two separate, discretized classifications, which may be causing information loss.

This work offers a foundational step towards developing more complex biophysical models of tongue that are able to encode higher level perceptible attributes such as stimulus compliance, surface roughness, movement velocity, and dynamic changes during the breakdown of food due to mastication. However, empirical biomechanical data and finite element models of the tongue are a prerequisite for this advancement.

Overall conclusions and future work

In this work, we developed predictive computational models that clarify the interplay of subtypes of sensory neural afferents, and their capacity to contribute to the neural encoding of stimulus diameter, contact geometry, and relative position. First, we employed differential equation models that abstract the neural biophysics in generating mechanosensitive currents and spike firing. Second, we built models of afferent population, varying in density, that encode spatial elements of stimuli such as diameter and contact geometry. Moreover, we leveraged machine learning approaches to classify stimulus spatial elements through their elicited afferent population responses.

Our efforts aim in the longer-term development of a computational platform to decode stimulus compliance, surface roughness, and lateral motion, via population response profiles of mechanosensitive afferents, as more layers of complexity in terms of stimulus contact mechanics with the simulated tongue become available. The grand aim of this effort is to provide the foundational steps in creating a computational platform, which can decode complex, non-linear percepts, e.g. firmness, smoothness, and thickness, but certain limitations exist in collecting in vivo neural and biomechanical data from tongue during oral processing of food. The overall scarcity of these data, and level of difficulty in collecting them present major challenges for developing models that are solely validated by tongue data. Using comparable information from cutaneous skin in other parts of the peripheral nervous system provides a viable path forward in building such computational models, until more data become available in tongue.

Summary of Findings and Contributions

Aim 1 Findings. Differentiated the contributions of SA and RA afferents in encoding food stimulus features during the first bite stage. The biophysical models developed recapitulated general spike firing patterns observed in microneurography recordings, validating their physiological relevance. The models showed that SA afferents are sensitive to stress magnitudes of ramp-and-hold stimuli, while RA afferents respond to the frequency and amplitude of periodic stimuli.

Aim 1 Contributions. A single-unit SA afferent model was adapted to function in response to both ramp-and-hold, and periodic stimuli, with direct comparison to similar microneurography data in the glabrous skin of the hand. Second, parameters were added to the generator function, which enabled a response to the onset and offset of stimuli, characteristic of RA afferent response profiles. These are the first single-unit computational models for SA and RA mechanosensitive afferents to be fitted to neural spike firing data in the human tongue. The contributions from **Aim 1** have been accepted for publication in the IEEE Engineering in Medicine and Biology Conference (IEEE EMBC, 2024).

Aim 2 Findings. Developed an afferent population model capable of encoding the geometry and diameter of food stimuli. The model demonstrated that population response metrics could effectively differentiate between blunt and curved stimuli across various diameters. The use of machine learning techniques enhanced the model's predictive capabilities, achieving high accuracy in classifying stimulus geometry and predicting diameter, while remaining insensitive to position modulation.

Aim 2 Contributions. Single-unit models developed in **Aim 1**, were adapted to become sensitive to spatial modulation of a stimulus that is not directly above their receptive field. Their responses were determined by the amount of normal stress the afferent was subjected to, according to its proximity from the stimulus edge (blunt stimulus) or center (curved stimulus). The mathematical form of the piecewise functions used to quantify this normal stress were presented in Eq. 1 and Eq. 2, for a blunt and curved stimulus, respectively. Second, these single unit models were distributed, according to a uniform probability density function, over a 50 x 25 mm two-dimensional simulated cross-section of the tongue. The total number of afferents in the population were optimized to minimize the amount of relative variance (coefficient of variation) elicited by spatial modulation of the stimulus center, to varying positions. This is the first computational population model, comprised of multiple afferent subtypes, specialized for the human tongue. Moreover, another novel contribution in this effort is the prediction of stimulus attributes, e.g. diameter and geometry, by synthesizing population responses from multiple afferent subtypes. The

contributions from **Aim 2** have been used to form a complete manuscript draft and will be submitted to the Journal of Texture Studies for publication.

Implications for Food Science and Industry. The insights gained from this research are relevant for the food industry, particularly in designing food products that better mimic the sensory experience of traditional foods, even when using alternative ingredients. Understanding how different textures are encoded by neural afferents can help create products that maintain consumer satisfaction, while paring the need for one-off perceptual evaluations.

Future Work

Incorporation of Additional Afferent Subtypes. Extend the model to include other mechanosensory afferents, such as those responding to lateral shear and movement velocity, to provide the basis for encoding motion of stimuli over the tongue. This would be especially important if lateral motion cannot be recapitulated with the current population model, which only receives normal stress tensors as input.

Clarifying Afferent Subtype Contributions in Predicting Stimulus Diameter and Geometry. In this effort, the population responses from both SA and RA afferents were used to discriminate stimulus diameter and geometry. However, it would be conducive to our understanding of neural encoding, to know exactly how much each afferent subtype contributes to these contributions, specifically when stimuli are varied in terms of their force magnitude and vibrational frequency. Moreover, whether predictions of stimulus attributes can reliably be made with small subsets of temporal data, e.g. during the first 100 ms of stimulus onset, as opposed to using all of the available data, at the aggregate level.

Exploration of Complex Stimuli. Investigate the neural encoding of higher-level physical attributes of stimuli, including varying compliance, surface roughness, as well as dynamic changes during mastication and food breakdown, to extend the model's applicability to real-world oral processing.

Application to Oral Processing Disorders. Use the findings to inform interventions for individuals with oral processing impairments. Developing assistive technologies or therapeutic strategies based on the neural encoding principles uncovered in this study could improve the quality of life for these individuals.

Publications

Accepted works

Conference Papers (Peer-reviewed publications)

1. **Rezaei, M.,** Guthrie, B., Gerling, G.J., "Biophysical models of slowly and rapidly adapting mechanosensitive tactile afferents in human tongue," 2024 IEEE Engineering in Medicine and Biology Conference (EMBC), 2024
2. **Rezaei, M.**, Nagi, S.S., Xu, C., McIntyre, S., Olausson, H., Gerling, G.J., "Thin Films on the Skin, but not Frictional Agents, Attenuate the Percept of Pleasantness to Brushed Stimuli," *2021 IEEE World Haptics Conference (WHC)*, Montreal, QC, Canada, 2021, pp. 49-54, doi: 10.1109/WHC49131.2021.9517259.

In progress works

Journal Papers

1. **Rezaei, M.,** Guthrie, B., Gerling, G.J., "Biophysical models of mechanosensitive tactile afferent populations in human tongue", (draft complete)
2. Xu, S., Hauser, S.C., Nagi, S.S., Jablonski, J.A, **Rezaei, M.**, Jarocka, E., Marshall, A.G., Olausson, H., McIntyre, S., Gerling, G.J., Mechanoreceptive A β primary afferents discriminate naturalistic social touch inputs at a functionally relevant time scale. bioRxiv, 2023.2007. 2022.549516 (2023)

References

[1] W. Xu, S. Yu, and M. Zhong, "A review on food oral tribology," *Friction*, vol. 10, no. 12, pp. 1927–1966, Dec. 2022, doi: 10.1007/s40544-022-0594-9.

[2] E. Çakır, C. J. Vinyard, G. Essick, C. R. Daubert, M. Drake, and E. A. Foegeding, "Interrelations among physical characteristics, sensory perception and oral processing of protein-based soft-solid structures," *Food Hydrocolloids*, vol. 29, no. 1, pp. 234–245, Oct. 2012, doi: 10.1016/j.foodhyd.2012.02.006.

[3] A. S. Szczesniak, "Texture is a sensory property," *Food Quality and Preference*, vol. 13, no. 4, pp. 215–225, Jun. 2002, doi: 10.1016/S0950-3293(01)00039-8.

[4] F. Lenfant, C. Loret, N. Pineau, C. Hartmann, and N. Martin, "Perception of oral food breakdown. The concept of sensory trajectory," *Appetite*, vol. 52, no. 3, pp. 659–667, Jun. 2009, doi: 10.1016/j.appet.2009.03.003.

[5] S. Fiszman and A. Tarrega, "The dynamics of texture perception of hard solid food: A review of the contribution of the temporal dominance of sensations technique," *Journal of Texture Studies*, vol. 49, no. 2, pp. 202–212, 2018, doi: 10.1111/jtxs.12273.

[6] A. Albert, A. Salvador, P. Schlich, and S. Fiszman, "Comparison between temporal dominance of sensations (TDS) and key-attribute sensory profiling for evaluating solid food with contrasting textural layers: Fish sticks," *Food Quality and Preference*, vol. 24, no. 1, pp. 111–118, Apr. 2012, doi: 10.1016/j.foodqual.2011.10.003.

[7] E. A. Foegeding, C. J. Vinyard, G. Essick, S. Guest, and C. Campbell, "Transforming Structural Breakdown into Sensory Perception of Texture," *Journal of Texture Studies*, vol. 46, no. 3, pp. 152–170, 2015, doi: 10.1111/jtxs.12105.

[8] E. Çakır, C. R. Daubert, M. A. Drake, C. J. Vinyard, G. Essick, and E. A. Foegeding, "The effect of microstructure on the sensory perception and textural characteristics of whey protein/κ-carrageenan

mixed gels," *Food Hydrocolloids*, vol. 26, no. 1, pp. 33–43, Jan. 2012, doi: 10.1016/j.foodhyd.2011.04.011.

[9] K. O. Johnson, "The roles and functions of cutaneous mechanoreceptors," *Current Opinion in Neurobiology*, vol. 11, no. 4, pp. 455–461, Aug. 2001, doi: 10.1016/S0959-4388(00)00234-8.

[10] V. E. Abraira and D. D. Ginty, "The Sensory Neurons of Touch," *Neuron*, vol. 79, no. 4, pp. 618–639, Aug. 2013, doi: 10.1016/j.neuron.2013.07.051.

[11] A. Zimmerman, L. Bai, and D. D. Ginty, "The gentle touch receptors of mammalian skin," *Science*, vol. 346, no. 6212, pp. 950–954, Nov. 2014, doi: 10.1126/science.1254229.

[12] R. S. Johansson and A. B. Vallbo, "Tactile sensibility in the human hand: relative and absolute densities of four types of mechanoreceptive units in glabrous skin.," *J Physiol*, vol. 286, pp. 283–300, Jan. 1979.

[13] A. B. Vallbo, K. E. Hagbarth, H. E. Torebjork, and B. G. Wallin, "Somatosensory, proprioceptive, and sympathetic activity in human peripheral nerves," *Physiological Reviews*, vol. 59, no. 4, pp. 919–957, Oct. 1979, doi: 10.1152/physrev.1979.59.4.919.

[14] M. Trulsson and G. K. Essick, "Low-threshold mechanoreceptive afferents in the human lingual nerve," *J Neurophysiol*, vol. 77, no. 2, pp. 737–748, Feb. 1997, doi: 10.1152/jn.1997.77.2.737.

[15] M. Trulsson and G. K. Essick, "Sensations Evoked by Microstimulation of Single Mechanoreceptive Afferents Innervating the Human Face and Mouth," *Journal of Neurophysiology*, vol. 103, no. 4, pp. 1741–1747, Apr. 2010, doi: 10.1152/jn.01146.2009.

[16] G. K. Essick and M. Trulsson, "Tactile Sensation in Oral Region," in *Encyclopedia of Neuroscience*, M. D. Binder, N. Hirokawa, and U. Windhorst, Eds., Berlin, Heidelberg: Springer, 2009, pp. 3999–4005. doi: 10.1007/978-3-540-29678-2_5872.

[17] M. Trulsson and R. S. Johansson, "Orofacial mechanoreceptors in humans: encoding characteristics and responses during natural orofacial behaviors," *Behavioural Brain Research*, vol. 135, no. 1, pp. 27–33, Sep. 2002, doi: 10.1016/S0166-4328(02)00151-1.

[18] A. Grigoriadis, A. Kumar, M. K. Åberg, and M. Trulsson, "Effect of Sudden Deprivation of Sensory Inputs From Periodontium on Mastication," *Front Neurosci*, vol. 13, p. 1316, Dec. 2019, doi: 10.3389/fnins.2019.01316.

[19] Y. Moayedi, S. Xu, S. K. Obayashi, B. U. Hoffman, G. J. Gerling, and E. A. Lumpkin, "In vivo calcium imaging identifies functionally and molecularly distinct subsets of tongue-innervating mechanosensory neurons," Neuroscience, preprint, Feb. 2022. doi: 10.1101/2022.02.11.480171.

[20] S. Maksimovic *et al.*, "Epidermal Merkel cells are mechanosensory cells that tune mammalian touch receptors," *Nature*, vol. 509, no. 7502, Art. no. 7502, May 2014, doi: 10.1038/nature13250.

[21] S. M. Maricich *et al.*, "Merkel cells are essential for light-touch responses," *Science*, vol. 324, no. 5934, pp. 1580–1582, Jun. 2009, doi: 10.1126/science.1172890.

[22] G. J. Gerling, L. Wan, B. U. Hoffman, Y. Wang, and E. A. Lumpkin, "Computation predicts rapidly adapting mechanotransduction currents cannot account for tactile encoding in Merkel cell-neurite complexes," *PLoS Comput Biol*, vol. 14, no. 6, p. e1006264, Jun. 2018, doi: 10.1371/journal.pcbi.1006264.

[23] D. R. Lesniak *et al.*, "Computation identifies structural features that govern neuronal firing properties in slowly adapting touch receptors," *eLife*, vol. 3, p. e01488, Jan. 2014, doi: 10.7554/eLife.01488.

[24] D. Deflorio, M. Di Luca, and A. M. Wing, "Skin and Mechanoreceptor Contribution to Tactile Input for Perception: A Review of Simulation Models," *Front Hum Neurosci*, vol. 16, p. 862344, Jun. 2022, doi: 10.3389/fnhum.2022.862344.

[25] S. S. Kim, A. P. Sripati, and S. J. Bensmaia, "Predicting the timing of spikes evoked by tactile stimulation of the hand," *J Neurophysiol*, vol. 104, no. 3, pp. 1484–1496, Sep. 2010, doi: 10.1152/jn.00187.2010.

[26] H. P. Saal, B. P. Delhaye, B. C. Rayhaun, and S. J. Bensmaia, "Simulating tactile signals from the whole hand with millisecond precision," *Proc. Natl. Acad. Sci. U.S.A.*, vol. 114, no. 28, Jul. 2017, doi: 10.1073/pnas.1704856114.

[27] V. B. Mountcastle, “Modality and topographic properties of single neurons of cat’s somatic sensory cortex,” *J Neurophysiol*, vol. 20, no. 4, pp. 408–434, Jul. 1957, doi: 10.1152/jn.1957.20.4.408.

[28] J. D. Greenspan and S. J. Bolanowski, “Chapter 2 - The Psychophysics of Tactile Perception and its Peripheral Physiological Basis,” in *Pain and Touch*, L. Kruger, Ed., in Handbook of Perception and Cognition. , San Diego: Academic Press, 1996, pp. 25–103. doi: 10.1016/B978-012426910-1/50004-2.

[29] B. Güçlü and S. J. Bolanowski, “Modeling population responses of rapidly-adapting mechanoreceptive fibers,” *J Comput Neurosci*, vol. 12, no. 3, pp. 201–218, 2002, doi: 10.1023/a:1016535413000.

[30] E. Hay and J. A. Pruszynski, “Orientation processing by synaptic integration across first-order tactile neurons,” *PLoS Comput Biol*, vol. 16, no. 12, p. e1008303, Dec. 2020, doi: 10.1371/journal.pcbi.1008303.

[31] G. J. Gerling, I. I. Rivest, D. R. Lesniak, J. R. Scanlon, and L. Wan, “Validating a population model of tactile mechanotransduction of slowly adapting type I afferents at levels of skin mechanics, single-unit response and psychophysics,” *IEEE Trans Haptics*, vol. 7, no. 2, pp. 216–228, 2014, doi: 10.1109/TOH.2013.36.

[32] Q. Ouyang, J. Wu, Z. Shao, D. Chen, and J. W. Bisley, “A Simplified Model for Simulating Population Responses of Tactile Afferents and Receptors in the Skin,” *IEEE Trans Biomed Eng*, vol. 68, no. 2, pp. 556–567, Feb. 2021, doi: 10.1109/TBME.2020.3007397.

[33] Y. Moayedi, S. Xu, S. K. Obayashi, B. U. Hoffman, G. J. Gerling, and E. A. Lumpkin, “The cellular basis of mechanosensation in mammalian tongue,” *Cell Reports*, vol. 42, no. 2, Feb. 2023, doi: 10.1016/j.celrep.2023.112087.

[34] R. S. Johansson, U. Landstro¨m, and R. Lundstro¨m, “Responses of mechanoreceptive afferent units in the glabrous skin of the human hand to sinusoidal skin displacements,” *Brain Research*, vol. 244, no. 1, pp. 17–25, Jul. 1982, doi: 10.1016/0006-8993(82)90899-X.

[35] K. O. Johnson, “Reconstruction of population response to a vibratory stimulus in quickly adapting mechanoreceptive afferent fiber population innervating glabrous skin of the monkey.,” *Journal of Neurophysiology*, vol. 37, no. 1, pp. 48–72, Jan. 1974, doi: 10.1152/jn.1974.37.1.48.

[36] A. Vallbo and R. S. Johansson, “Properties of cutaneous mechanoreceptors in the human hand related to touch sensation,” *Hum Neurobiol*, vol. 3, no. 1, Art. no. 1, 1984.

[37] M. Trulsson and G. K. Essick, “Low-Threshold Mechanoreceptive Afferents in the Human Lingual Nerve,” *Journal of Neurophysiology*, vol. 77, no. 2, pp. 737–748, Feb. 1997, doi: 10.1152/jn.1997.77.2.737.

[38] E. Lauga, C. J. Pipe, and B. Le Révérend, “Sensing in the Mouth: A Model for Filiform Papillae as Strain Amplifiers,” *Frontiers in Physics*, vol. 4, 2016, Accessed: Dec. 28, 2023. [Online]. Available: https://www.frontiersin.org/articles/10.3389/fphy.2016.00035

[39] V. J. Napadow, Q. Chen, V. J. Wedeen, and R. J. Gilbert, “Intramural mechanics of the human tongue in association with physiological deformations,” *Journal of Biomechanics*, vol. 32, no. 1, pp. 1–12, Jan. 1999, doi: 10.1016/S0021-9290(98)00109-2.

[40] D. Wang, C. He, C. Wu, and Y. Zhang, “Mechanical behaviors of tension and relaxation of tongue and soft palate: Experimental and analytical modeling,” *Journal of Theoretical Biology*, vol. 459, pp. 142–153, Dec. 2018, doi: 10.1016/j.jtbi.2018.10.001.

[41] J. Chen, R. Ahmad, W. Li, M. Swain, and Q. Li, “Biomechanics of oral mucosa,” *J R Soc Interface*, vol. 12, no. 109, p. 20150325, Aug. 2015, doi: 10.1098/rsif.2015.0325.

[42] Y. Dong, S. Mihalas, S. S. Kim, T. Yoshioka, S. Bensmaia, and E. Niebur, “A simple model of mechanotransduction in primate glabrous skin,” *Journal of Neurophysiology*, vol. 109, no. 5, pp. 1350–1359, Mar. 2013, doi: 10.1152/jn.00395.2012.

[43] Y. Moayedi, S. Michlig, M. Park, A. Koch, and E. A. Lumpkin, “Somatosensory innervation of healthy human oral tissues,” *Journal of Comparative Neurology*, vol. 529, no. 11, pp. 3046–3061, 2021, doi: 10.1002/cne.25148.

[44] M. Condon *et al.*, “Differential sensitivity to surface compliance by tactile afferents in the human finger pad,” *Journal of Neurophysiology*, vol. 111, no. 6, pp. 1308–1317, Mar. 2014, doi: 10.1152/jn.00589.2013.

[45] C. Xu, Y. Wang, and G. J. Gerling, “An elasticity-curvature illusion decouples cutaneous and proprioceptive cues in active exploration of soft objects,” *PLOS Computational Biology*, vol. 17, no. 3, p. e1008848, Mar. 2021, doi: 10.1371/journal.pcbi.1008848.

[46] M. G. Aguayo-Mendoza, E. C. Ketel, E. van der Linden, C. G. Forde, B. Piqueras-Fiszman, and M. Stieger, “Oral processing behavior of drinkable, spoonable and chewable foods is primarily determined by rheological and mechanical food properties,” *Food Quality and Preference*, vol. 71, pp. 87–95, Jan. 2019, doi: 10.1016/j.foodqual.2018.06.006.

[47] R. Di Monaco, N. A. Miele, S. Volpe, P. Masi, and S. Cavella, “Temporal dominance of sensations and dynamic liking evaluation of polenta sticks,” *British Food Journal*, vol. 118, no. 3, pp. 749–760, Jan. 2016, doi: 10.1108/BFJ-07-2015-0236.

[48] D. Deflorio, M. Di Luca, and A. M. Wing, “Skin and Mechanoreceptor Contribution to Tactile Input for Perception: A Review of Simulation Models,” *Front Hum Neurosci*, vol. 16, p. 862344, Jun. 2022, doi: 10.3389/fnhum.2022.862344.

[49] F. Pastor *et al.*, “Bayesian and Neural Inference on LSTM-Based Object Recognition From Tactile and Kinesthetic Information,” *IEEE Robotics and Automation Letters*, vol. 6, no. 1, pp. 231–238, Jan. 2021, doi: 10.1109/LRA.2020.3038377.

[50] H. Tan *et al.*, “Tactile sensory coding and learning with bio-inspired optoelectronic spiking afferent nerves,” *Nat Commun*, vol. 11, no. 1, p. 1369, Mar. 2020, doi: 10.1038/s41467-020-15105-2.

[51] S. Ostojic and N. Brunel, “From Spiking Neuron Models to Linear-Nonlinear Models,” *PLOS Computational Biology*, vol. 7, no. 1, p. e1001056, Jan. 2011, doi: 10.1371/journal.pcbi.1001056.

[52] E. J. Chichilnisky, “A simple white noise analysis of neuronal light responses,” *Network*, vol. 12, no. 2, pp. 199–213, May 2001.

[53] M. Krumin and S. Shoham, “Multivariate Autoregressive Modeling and Granger Causality Analysis of Multiple Spike Trains,” *Comput Intell Neurosci*, vol. 2010, p. 752428, 2010, doi: 10.1155/2010/752428.

[54] G. Corniani, M. A. Casal, S. Panzeri, and H. P. Saal, “Population coding strategies in human tactile afferents,” *PLOS Computational Biology*, vol. 18, no. 12, p. e1010763, Dec. 2022, doi: 10.1371/journal.pcbi.1010763.

[55] F. Pei *et al.*, “Neural Latents Benchmark ’21: Evaluating latent variable models of neural population activity.” arXiv, Jan. 17, 2022. doi: 10.48550/arXiv.2109.04463.

[56] A. C. Smith and E. N. Brown, “Estimating a state-space model from point process observations,” *Neural Comput*, vol. 15, no. 5, pp. 965–991, May 2003, doi: 10.1162/089976603765202622.

[57] B. M. Yu, J. P. Cunningham, G. Santhanam, S. I. Ryu, K. V. Shenoy, and M. Sahani, “Gaussian-Process Factor Analysis for Low-Dimensional Single-Trial Analysis of Neural Population Activity,” *J Neurophysiol*, vol. 102, no. 1, pp. 614–635, Jul. 2009, doi: 10.1152/jn.90941.2008.

[58] R. Quian Quiroga and S. Panzeri, “Extracting information from neuronal populations: information theory and decoding approaches,” *Nat Rev Neurosci*, vol. 10, no. 3, pp. 173–185, Mar. 2009, doi: 10.1038/nrn2578.

[59] A. Pouget, P. Dayan, and R. Zemel, “Information processing with population codes,” *Nat Rev Neurosci*, vol. 1, no. 2, pp. 125–132, Nov. 2000, doi: 10.1038/35039062.

[60] G. J. Gerling and G. W. Thomas, “Fingerprint lines may not directly affect SA-I mechanoreceptor response,” *Somatosensory & Motor Research*, vol. 25, no. 1, pp. 61–76, Mar. 2008, doi: 10.1080/08990220701838996.

[61] J. R. Phillips and K. O. Johnson, “Tactile spatial resolution. II. Neural representation of Bars, edges, and gratings in monkey primary afferents,” *Journal of Neurophysiology*, vol. 46, no. 6, pp. 1192–1203, Dec. 1981, doi: 10.1152/jn.1981.46.6.1192.

[62] G. Corniani and H. P. Saal, “Tactile innervation densities across the whole body,” Neuroscience, preprint, Apr. 2020. doi: 10.1101/2020.04.27.063263.